Effects of spin–orbit coupling on magnetic properties of discrete and extended magnetic systems

ARTICLE *in* JOURNAL OF COMPUTATIONAL CHEMISTRY · OCTOBER 2008

Impact Factor: 3.59 · DOI: 10.1002/jcc.21011 · Source: PubMed

3 AUTHORS, INCLUDING:

H. J. Xiang
Fudan University
156 PUBLICATIONS **3,370** CITATIONS
SEE PROFILE

Myung-Hwan Whangbo
North Carolina State University
703 PUBLICATIONS **14,870** CITATIONS
SEE PROFILE

Effects of Spin-Orbit Coupling on Magnetic Properties of Discrete and Extended Magnetic Systems

DADI DAI,* HONGJUN XIANG,† MYUNG-HWAN WHANGBO
Department of Chemistry, North Carolina State University, Raleigh, North Carolina 27695-8204

Received 30 January 2008; Revised 16 March 2008; Accepted 25 March 2008
DOI 10.1002/jcc.21011
Published online in Wiley InterScience (www.interscience.wiley.com).

Abstract: In accounting for the magnetic properties of discrete and extended compounds with unpaired spins, it is crucial to know the nature of their ground and low-lying excited states. In this review we surveyed quantum mechanical descriptions on how these states are affected by spin-orbit coupling and attempted to provide a conceptual framework with which to think about spin-orbit coupling and its applications.

 J Comput Chem 00: 000–000, 2008

Key words: spin-orbit coupling; magnetic properties; spin angular momentum; orbital angular momentum

Introduction

Discrete and extended solids containing unpaired spins have low-lying excited states with different spin moments and hence exhibit a variety of interesting magnetic properties. The energy states of a magnetic system are commonly described in terms of crystal field splitting, spin exchange interaction, and spin-orbit coupling. In general, crystal field splitting and spin exchange interaction are strong compared with spin-orbit coupling interactions. Thus, one normally examines how spin-orbit coupling affects the energy states of a magnetic system determined by crystal field splitting and spin exchange interaction. Nevertheless, spin-orbit coupling plays a crucial role in explaining the magnetic properties of compounds with unpaired spins. In this review we survey important theoretical and conceptual developments on spin-orbit coupling and its applications.

Spin-Orbit Coupling Constant

The experimentally observed magnetic moment is associated with the total angular momentum $\vec{J}$, which is the vector sum of an orbital angular momentum $\vec{L}$ and a spin angular momentum $\vec{S}$, i.e., $\vec{J} = \vec{L} + \vec{S}$. In relativistic quantum mechanics, the experimentally deduced $\vec{J}$ cannot be partitioned into $\vec{L}$ and $\vec{S}$ contributions, because the operators $\hat{L}$ and $\hat{S}$ do not commute with the relativistic Hamiltonian $\hat{H}_{\mathrm{R}}$. In nonrelativistic quantum mechanics, however, the operators $\hat{L}$ and $\hat{S}$ commute with the nonrelativistic Hamiltonian $\hat{H}_{\mathrm{NR}}$, so the two types of angular momenta are well distinguished. Even when the relativistic effect is not negligible, one can still use $\vec{L}$ and $\vec{S}$ as long as the coupling between the two angular momenta, i.e., spin-orbit coupling, is properly taken into consideration. Spin-orbit coupling arises naturally as a consequence of relativistic quantum mechanics, in which $\hat{H}_{\mathrm{R}}$ is described by the Dirac equation. In the limit of $c \to \infty$, $\hat{H}_{\mathrm{R}}$ is transformed into $\hat{H}_{\mathrm{NR}}$ plus a few energy terms including spin-orbit coupling.

In classical mechanics the energy of interaction between the orbital and spin moments of an electron in a given atom is written as[1]

$$E = \xi(r)\vec{S} \cdot \vec{L}, \tag{1}$$

where $\xi(r)$ is a constant, which increases with the nuclear charge of the atom and decreases with the radius r of the electron moving around the nucleus. Given the distribution of an electron, the spin-orbit coupling constant $\langle\xi\rangle$ of the atom is obtained by integrating $\xi(r)$ over the radial wavefunction $R(r)$, i.e.,

$$\langle\xi\rangle = \int_0^\infty \xi(r)[R(r)]^2 r^2 dr\,. \tag{2}$$

By analogy to eq. (1), the spin-orbit coupling energy for an atom with many unpaired electrons and total spin S is expressed as

*Present address: Duke Clinical Research Institute, Durham, North Carolina 27705

†Present address: National Renewable Energy Laboratory, Golden, Colorado 80401

Correspondence to: M.-H. Whangbo; e-mail: mike_whangbo@ncsu.edu

Contract/grant sponsor: Office of Basic Energy Sciences, Division of Materials Sciences, US Department of Energy; Contract/grant number: DE-FG02-86ER45259

Table 1. Extrapolated Values (in cm^{-1}) of the Single Electron Spin-Orbit Coupling Constants $\langle\xi\rangle$ for 3d and 4d Transition-Metal Elements as a Function of Their Oxidation States (Reproduced from ref. 3).[a]

	M^0	M^+	M^{2+}	M^{3+}	M^{4+}	M^{5+}	M^{6+}
Ti	70	90	120	155			
V	(95)	135	170	210	250		
Cr	(135)	(190)	230	275	325	380	
Mn	(190)	255	(300)	355	415	475	540
Fe	255	345	400	(460)	515	555	665
Co	390	455	515	(580)	(650)	715	790
Ni		605	630	(715)	(790)	(865)	950
Cu			830	(875)	(960)	(1030)	(1130)
Zr	270	340	425	500			
Nb	(365)	490	555	670	750		
Mo	(450)	(630)	(695)	820	950	1030	
Tc	(550)	740	(850)	(990)	(1150)	(1260)	1450
Ru	745	900	1000	(1180)	(1350)	(1500)	(1700)
Rh	940	1060	1220	(1360)	(1570)	(1730)	(1950)
Pd		1420	1460	(1640)	(1830)	(2000)	(2230)
Ag			1840	(1930)	(2100)	(2300)	(2500)

[a]The values in parentheses are experimentally observed.

$$E_{SO} = \lambda \vec{S} \cdot \vec{L}, \tag{3}$$

where λ is the spin-orbit coupling constant.

$$\lambda = \langle\xi\rangle/2S. \tag{4}$$

This constant λ is positive when the electron shell containing unpaired electrons is less than half-filled as in, e.g., V^{4+} (d^1). For the case of $\lambda > 0$, the lowest-energy spin-orbit coupled state is obtained when $\vec{L}$ and $\vec{S}$ are antiparallel with $\vec{J} = \vec{L} - \vec{S}$. However, the constant λ is negative if the shell is more than half-filled as in, e.g., Cu^{2+} (d^9). For the case of $\lambda < 0$, the lowest-energy spin-orbit coupled state is obtained when $\vec{L}$ and $\vec{S}$ are parallel with $\vec{J} = \vec{L} + \vec{S}$. If the shell is half filled as in, e.g., high-spin Mn^{2+} (d^5), spin-orbit coupling vanishes because $\vec{L} = 0$ for such an ion. The values of $\langle\xi\rangle$ for 3d and 4d transition-metal ions calculated and/or observed as a function of their oxidation state[1,2] are reproduced in Table 1. For a given oxidation state, the $\langle\xi\rangle$ value of an element increases with increasing the atomic number. For a given element, the $\langle\xi\rangle$ value increases with increasing the oxidation state.

Electronic Structure and Orbital Angular Momentum

The magnetic moment $\vec{\mu}$ of a system is measured as the change of its total energy E with respect to the variation of the applied magnetic field $\vec{H}$, namely,

$$\vec{\mu} = -\frac{\partial E}{\partial \vec{H}}. \tag{5}$$

It is recalled that the angular momentum $\vec{L}$ is proportional to $\vec{\mu}$ as

$$\vec{\mu} = -\mu_B \vec{L}, \tag{6}$$

where μ_B is the Bohr magneton ($\mu_B H \approx 5.8 \times 10^{-5}$ eV at the magnetic field $H = 1$ T). (To be precise, the symbol $\vec{L}$ refers to the orbital angular momentum. In this general discussion, however, $\vec{L}$ may refer to any kind of angular momentum, namely, the orbital, the spin or the total angular momentum.) To measure the magnetic moment along a certain direction, one applies an external magnetic field along that direction and measure the energy change, i.e.,

$$\vec{L} = \frac{\partial E}{\mu_B \partial \vec{H}}. \tag{7}$$

Equations (6) and (7) are the starting point of our discussion on how electronic structure is related to orbital angular momentum and hence magnetic properties.

Systems With One Singly Occupied Orbital

For a system with a single electron, the total energy is simply the energy of the occupied orbital. To calculate the orbital angular momentum of such a system, it is necessary to construct the matrix representation of an appropriate Hamiltonian and diagonalize it. Application of a magnetic field $\vec{H}$ gives rise to the Zeeman operator $\hat{H}_Z$,

$$\hat{H}_Z = -\vec{\mu}_L \cdot \vec{H} = \mu_B \hat{L} \cdot \vec{H} = \mu_B \hat{L}_x H_x + \mu_B \hat{L}_y H_y + \mu_B \hat{L}_z H_z. \tag{8}$$

As a specific example, consider the case when one electron is present in one of the three p orbitals, p_i ($i = x, y, z$). The effective one-electron Hamiltonian $\hat{H}^{eff}$ of this system satisfies

$$\hat{H}^{eff} p_i = \varepsilon_i p_i \qquad (i = x, y, z), \tag{9}$$

where ε_x, ε_y, and ε_z are the energies of the orbitals p_x, p_y, and p_z, respectively. This system under a magnetic field is described by the Hamiltonian $\hat{H} = \hat{H}^{eff} + \hat{H}_Z$. Then, by using the integrals of $\hat{L}|p_i\rangle$ listed in Table 2, the matrix representation of $\hat{H}$ in terms of the three orbitals p_x, p_y, and p_z, i.e., $\langle p_i|\hat{H}|p_j\rangle$ ($i, j = x, y, z$), is obtained as

Table 2. Values of the Integrals $<p_i|\hat{L}_\mu|p_j>$ for Atomic p Orbitals (i, j = x, y, z).

	$\|p_x>$	$\|p_y>$	$\|p_z>$
$\hat{L}_\mu = \hat{L}_x$			
$<p_x\|$	0	0	0
$<p_y\|$	0	0	−i
$<p_z\|$	0	i	0
$\hat{L}_\mu = \hat{L}_y$			
$<p_x\|$	0	0	i
$<p_y\|$	0	0	0
$<p_z\|$	−i	0	0
$\hat{L}_\mu = \hat{L}_z$			
$<p_x\|$	0	−i	0
$<p_y\|$	i	0	0
$<p_z\|$	0	0	0

$$\mathbf{H} = \begin{pmatrix} \varepsilon_x & -i\mu_B H_z & i\mu_B H_y \\ i\mu_B H_z & \varepsilon_y & -i\mu_B H_x \\ -i\mu_B H_y & i\mu_B H_x & \varepsilon_z \end{pmatrix}. \quad (10)$$

When the field is applied along the z-direction so that $H_x = H_y = 0$, the above expression becomes

$$\mathbf{H} = \begin{pmatrix} \varepsilon_x & -i\mu_B H_z & 0 \\ i\mu_B H_z & \varepsilon_y & 0 \\ 0 & 0 & \varepsilon_z \end{pmatrix}. \quad (11)$$

The diagonalization of this matrix leads to three energies

$$\begin{aligned} E_1 &= \frac{(\varepsilon_x + \varepsilon_y) - \sqrt{(\varepsilon_x - \varepsilon_y)^2 + 4\mu_B^2 H_z^2}}{2}, \\ E_2 &= \frac{(\varepsilon_x + \varepsilon_y) + \sqrt{(\varepsilon_x - \varepsilon_y)^2 + 4\mu_B^2 H_z^2}}{2}, \\ E_3 &= \varepsilon_z. \end{aligned} \quad (12)$$

Note that $E_1 < E_2$. Consequently, if $E_1 < E_3$, the ground state is given by E_1. Therefore, for the ground state, the orbital angular momentum of the single electron is given by

$$L_z = \frac{\partial E_1}{\mu_B \partial H_z} = \frac{-2\mu_B H_z}{\sqrt{(\varepsilon_x - \varepsilon_y)^2 + 4\mu_B^2 H_z^2}}. \quad (13)$$

Thus, if the p_x and p_y levels are degenerate (i.e., if $\varepsilon_x = \varepsilon_y$), the L_z value becomes -1 in units of $\hbar$. The degeneracy of the p_x and p_y levels is lifted when the symmetry of the system holding the electron is lowered. In such a case, the energy difference $|\varepsilon_x - \varepsilon_y|$ is generally much greater than $\mu_B H_z$, because the latter term is small (Recall that $\mu_B H \approx 5.8 \times 10^{-5}$ eV at $H = 1$ T). As a result,

$$L_z = -\frac{2\mu_B H_z}{|\varepsilon_x - \varepsilon_y|}, \quad (14)$$

which is much smaller than -1 in magnitude. This is an example of orbital momentum quenching caused by the removal of orbital degeneracy. Finally, consider that $E_3 < E_1$, so the ground state is given by E_3. In this case, the orbital angular momentum of the system is zero, because its energy does not depend on the applied field.

The above procedure of calculating the orbital angular momentum can be readily extended to a more general one-electron system described by one-electron orbitals ψ_i with energies ε_i ($i = 1, 2, \ldots, m$):

a. Calculate the matrix elements $\langle \psi_i | \hat{H}_Z | \psi_j \rangle$ ($i, j = 1, 2, \ldots, m$) to obtain the $m \times m$ matrix representation of $\hat{H}_Z$.
b. Add the orbital energy ε_i to the i-th diagonal element of this matrix to obtain the matrix representation of the Hamiltonian $\hat{H} = \hat{H}^{\text{eff}} + \hat{H}_Z$.
c. Diagonalize the resulting matrix to obtain the eigenvalues of $\hat{H}$.
d. Calculate the derivatives of the eigenvalues with respect to the magnetic field $\vec{H}$ to obtain the orbital angular momentum associated with the eigenstates. In general, the angular momentum of the ground state is most important to consider.

Systems With Many Singly Occupied Orbitals

To describe a system with more than one unpaired electron, it is necessary to employ the electronic states of the system rather than the one-electron orbitals as the bases for obtaining the matrix representation of the Hamiltonian $\hat{H}_Z$. For example, the ground state of a free Co^{3+} (d^6) ion is ^5D (i.e., $L = 2$, $S = 2$). In the absence of spin-orbit coupling, the orbital states can be denoted by the functions $|LM_L\rangle$, i.e., $|2 \pm 2\rangle$, $|2 \pm 1\rangle$, and $|20\rangle$. In terms of the orbital angular momentum operators, the orbital states $|LM_L\rangle$ satisfy the following relationships:

$$\begin{aligned} \hat{L}_x|LM_L\rangle &= (1/2)(\hat{L}_+ + \hat{L}_-)|LM_L\rangle, \\ \hat{L}_y|LM_L\rangle &= (1/2i)(\hat{L}_+ - \hat{L}_-)|LM_L\rangle, \end{aligned} \quad (15)$$

$$\hat{L}_z|LM_L\rangle = M_L|LM_L\rangle, \quad (16)$$

$$\begin{aligned} \hat{L}_+|LM_L\rangle &= \sqrt{(L + M_L + 1)(L - M_L)}|LM_L + 1\rangle, \\ \hat{L}_-|LM_L\rangle &= \sqrt{(L - M_L + 1)(L + M_L)}|LM_L - 1\rangle, \end{aligned} \quad (17)$$

Thus, one can easily calculate all the required matrix elements $\langle LM_L|\hat{H}_z|L'M_{L'}\rangle$. For the free ion, the five components of the D state are degenerate so that the states $|LM_L\rangle$ have the same energy, and hence it is not necessary to add these energies to the diagonal elements $\langle LM_L|\hat{H}_z|LM_L\rangle$. However, if the cation is placed under a certain crystal field, the associated symmetry lowering lifts the degeneracy of the states $|LM_L\rangle$ so that their energies are not identical any more. For example, the ^5D state of a high-spin Fe^{2+} (d^6) ion at a linear two-coordinate site splits into three different energy levels, namely, $|2 \pm 2\rangle$ at energy E_2, $|2 \pm 1\rangle$ at energy E_1, and $|20\rangle$ at energy E_0, with $E_2 < E_1 < E_0$ (see "High-spin d^6 ions at trigonal prism and linear two coordinate sites" section).[3] As a consequence, the state energies E_2, E_1, and E_0 should be added to the diagonal elements $\langle LM_L|\hat{H}_z|LM_L\rangle$ for the states $|2 \pm 2\rangle$, $|2 \pm 1\rangle$, and $|20\rangle$, respectively, in order to obtain the matrix representation of the Hamiltonian $\hat{H} = \hat{H}^{\text{eff}} + \hat{H}_Z$ for a system under magnetic field.

When the ground state is nondegenerate, the description of electronic structure can be simplified in terms of one-electron orbitals. For example, consider a Cu^{2+} (d^9) ion at an axially elongated octahedral site in which the fourfold rotational axis is taken as the z-axis (Fig. 1a). Then, in the ground state, the highest-lying d-block level $x^2 - y^2$ is singly occupied, and the remaining d-block levels are doubly occupied (Fig. 1b). (It should be noted that, in each the d-block level of Cu^{2+}, the 3d-orbital of Cu is combined out-of-phase with the p orbitals of the surrounding ligand atoms. For convenience, each d-block level is identified by referring only to the 3d-orbital of Cu.) Thus the ground electronic state of a Cu^{2+} (d^9) ion can be described by the configuration

$$\Phi_G = (xy)^2(xz)^2(yz)^2(z^2)^2(x^2 - y^2)^1, \quad (18)$$

which has a "hole" in the $x^2 - y^2$ level. The excited electronic states of this cation are given by the configurations in which holes are present in other d-block levels, namely,

$$\begin{aligned}\Phi_1 &= (xy)^2(xz)^2(yz)^2(z^2)^1(x^2{-}y^2)^2,\\ \Phi_2 &= (xy)^2(xz)^2(yz)^1(z^2)^2(x^2{-}y^2)^2,\\ \Phi_3 &= (xy)^2(xz)^1(yz)^2(z^2)^2(x^2{-}y^2)^2,\\ \Phi_4 &= (xy)^1(xz)^2(yz)^2(z^2)^2(x^2-y^2)^2.\end{aligned} \tag{19}$$

Now, consider the matrix elements $\langle\Phi_m|\hat{L}|\Phi_n\rangle$, which is written as

$$\langle\Phi_m|\hat{L}|\Phi_n\rangle = \sum_{i=1}^{9}\langle\Phi_m|\hat{L}(i)|\Phi_n\rangle,$$

where $\hat{L}(i)$ denotes the angular momentum operator for the nine d-electron $i = 1, 2, \ldots, 9$ of Cu^{2+}. The integral $\langle\Phi_m|\hat{L}(i)|\Phi_n\rangle$ vanishes when the Slater determinant Φ_m differs from Φ_n by more than one orbital, and is equal to $\langle\phi_m(i)|\hat{L}(i)|\phi_n(i)\rangle$ if $\phi_m(i)$ of Φ_m is the only orbital that is different from $\phi_n(i)$ of Φ_n. For the d orbitals ϕ_i, the values of $\hat{L}|\phi_i\rangle$ are summarized in Table 3. Using this result, the matrix elements $\langle\Phi_m|\hat{H}_Z|\Phi_n\rangle$ are evaluated as

$$\begin{aligned}\langle\Phi_G|\mu_B\hat{L}\cdot\vec{H}|\Phi_1\rangle &= \langle x^2-y^2(i)|\mu_B\hat{L}(i)\cdot\vec{H}|z^2(i)\rangle = 0\\ \langle\Phi_G|\mu_B\hat{L}\cdot\vec{H}|\Phi_2\rangle &= \langle x^2-y^2(i)|\mu_B\hat{L}(i)\cdot\vec{H}|yz(i)\rangle = -i\mu_B H_x\\ \langle\Phi_G|\mu_B\hat{L}\cdot\vec{H}|\Phi_3\rangle &= \langle x^2-y^2(i)|\mu_B\hat{L}(i)\cdot\vec{H}|xz(i)\rangle = -i\mu_B H_y\\ \langle\Phi_G|\mu_B\hat{L}\cdot\vec{H}|\Phi_4\rangle &= \langle x^2-y^2(i)|\mu_B\hat{L}(i)\cdot\vec{H}|xy(i)\rangle = 2i\mu_B H_z\end{aligned} \tag{20}$$

For simplicity of our discussion, we introduce the following notations:

$$\begin{aligned}(x^2-y^2||z^2) &\equiv \langle\Phi_G|\mu_B\hat{L}\cdot\vec{H}|\Phi_1\rangle = (z^2||x^2-y^2)*,\\ (x^2-y^2||yz) &\equiv \langle\Phi_G|\mu_B\hat{L}\cdot\vec{H}|\Phi_2\rangle = (yz||x^2-y^2)*,\\ (x^2-y^2||xz) &\equiv \langle\Phi_G|\mu_B\hat{L}\cdot\vec{H}|\Phi_3\rangle = (xz||x^2-y^2)*,\\ (x^2-y^2||xy) &\equiv \langle\Phi_G|\mu_B\hat{L}\cdot\vec{H}|\Phi_4\rangle = (xy||x^2-y^2)*,\end{aligned} \tag{21}$$

where the symbols "*" indicate the complex conjugates of the matrix elements under consideration. The energy difference between the ground state and the excited states is generally much greater than $\mu_B H$. Thus, the lowest eigenvalue is well approximated by employing the second-order perturbation theory, which leads to

$$\begin{aligned}E &= -\frac{|(x^2-y^2||z^2)|^2}{E_1-E_0} - \frac{|(x^2-y^2||yz)|^2}{E_2-E_0} - \frac{|(x^2-y^2||xz)|^2}{E_3-E_0}\\ &\quad - \frac{|(x^2-y^2||xy)|^2}{E_4-E_0}\\ &= 0 - \frac{(\mu_B H_x)^2}{E_2-E_0} - \frac{(\mu_B H_y)^2}{E_3-E_0} - \frac{4(\mu_B H_z)^2}{E_4-E_0}.\end{aligned} \tag{22}$$

Then, by using eq. (7), we have the orbital angular momentum for the ground state

Table 3. Values of the Integrals $\langle d_i|\hat{L}_\mu|d_j\rangle$ for Atomic d Orbitals ($i, j = z^2, x^2-y^2$, xy, yz, xz).

	$\|d_{z2}\rangle$	$\|d_{x2-y2}\rangle$	$\|d_{xy}\rangle$	$\|d_{yz}\rangle$	$\|d_{xz}\rangle$
$\hat{L}_\mu = \hat{L}_x$					
$\langle d_{z2}\|$	0	0	0	$i\sqrt{3}$	0
$\langle d_{x2-y2}\|$	0	0	0	i	0
$\langle d_{xy}\|$	0	0	0	0	$-i$
$\langle d_{yz}\|$	$-i\sqrt{3}$	$-i$	0	0	0
$\langle d_{xz}\|$	0	0	i	0	0
$\hat{L}_\mu = \hat{L}_y$					
$\langle d_{z2}\|$	0	0	0	0	$-i\sqrt{3}$
$\langle d_{x2-y2}\|$	0	0	0	0	i
$\langle d_{xy}\|$	0	0	0	I	0
$\langle d_{yz}\|$	0	0	$-i$	0	0
$\langle d_{xz}\|$	$i\sqrt{3}$	$-i$	0	0	0
$\hat{L}_\mu = \hat{L}_z$					
$\langle d_{z2}\|$	0	0	0	0	0
$\langle d_{x2-y2}\|$	0	0	$-2i$	0	0
$\langle d_{xy}\|$	0	2i	0	0	0
$\langle d_{yz}\|$	0	0	0	0	i
$\langle d_{xz}\|$	0	0	0	$-i$	0

$$\vec{L} = -\frac{2\mu_B H_x}{E_2-E_0}\hat{x} - \frac{2\mu_B H_y}{E_3-E_0}\hat{y} - \frac{8\mu_B H_z}{E_4-E_0}\hat{z}. \tag{23}$$

In general, the orbital angular momentum for a nondegenerate ground state may be written as

$$\begin{aligned}\vec{L} = \sum_n^{\text{excited states}}\Bigg(&-\frac{2\mu_B H_x|<\psi_0|\hat{L}_x|\psi_n>|^2}{E_n-E_0}\hat{x}\\ &-\frac{2\mu_B H_y|<\psi_0|\hat{L}_y|\psi_n>|^2}{E_n-E_0}\hat{y} - \frac{2\mu_B H_z|<\psi_0|\hat{L}_z|\psi_n>|^2}{E_0-E_n}\hat{z}\Bigg)\end{aligned} \tag{24}$$

If we define

$$\begin{aligned}\Lambda_{xx} &= \sum_n^{\text{excited states}}\frac{|<\psi_0|\hat{L}_x|\psi_n>|^2}{E_n-E_0},\\ \Lambda_{yy} &= \sum_n^{\text{excited states}}\frac{|<\psi_0|\hat{L}_y|\psi_n>|^2}{E_n-E_0},\\ \Lambda_{zz} &= \sum_n^{\text{excited states}}\frac{|<\psi_0|\hat{L}_z|\psi_n>|^2}{E_n-E_0},\end{aligned} \tag{25}$$

the orbital angular momentum associated with the nondegenerate ground state is written as

$$\vec{L} = -2\mu_B(\Lambda_{xx}H_x\,\hat{x} + \Lambda_{yy}H_y\,\hat{y} + \Lambda_{zz}H_z\hat{z}). \tag{26}$$

Therefore, the quantity $2\mu_B\Lambda_{\mu\mu}H_\mu$ represents the unquenched orbital angular momentum along the direction $\mu = x, y, z$. In the

above example of a Cu^{2+} (d^9) ion, it is seen from eqs. (23) and (26) that

$$\Lambda_{xx} = \frac{1}{E_2 - E_0}, \quad \Lambda_{yy} = \frac{1}{E_3 - E_0}, \quad \Lambda_{zz} = \frac{4}{E_4 - E_0}. \tag{27}$$

When the ground orbital state of a system is degenerate, the description of the electronic state requires a linear combination of several configurations (i.e., Slater determinants), so that it is necessary to construct and diagonalize the matrix representation of its Hamiltonian under an external magnetic field (see "High-spin d^6 ions at trigonal prism and linear two coordinate sites" section for further discussion). As a consequence, there is no general analytical expression for the orbital angular momentum of such a system.

Effect of Spin-Orbit Coupling on a Single Spin Site and Magnetic Anisotropy

The effect of spin-orbit coupling on a single spin site is basically described by considering the zero-field splitting and the deviation of g-factor from the value of 2. Let us start with the combined Hamiltonian of the spin-orbit coupling and the Zeeman term,

$$\hat{H}' = \hat{H}_{SO} + \hat{H}_Z = \lambda \hat{L} \cdot \hat{S} + \mu_B (\hat{L} + 2\hat{S}) \cdot \vec{H}. \tag{28}$$

To obtain the eigenvalues and eigenfunctions of $\hat{H}'$, one needs to construct the Hamiltonian matrix using the basis functions $|LM_L\rangle|SM_S\rangle$, i.e., the product of the orbital state $|LM_L\rangle$ and the spin state $|SM_S\rangle$. In terms of the spin momentum operators, the spin states $|SM_S\rangle$ satisfy the relationships:

$$\begin{aligned} \hat{S}_x|SM_S\rangle &= (1/2)\big(\hat{S}_+ + \hat{S}_-\big)|SM_S\rangle, \\ \hat{S}_y|SM_S\rangle &= (1/2i)\big(\hat{S}_+ - \hat{S}_-\big)|SM_S\rangle, \end{aligned} \tag{29}$$

$$\hat{S}_z|SM_S\rangle = M_S|SM_S\rangle, \tag{30}$$

$$\begin{aligned} \hat{S}_+|SM_S\rangle &= \sqrt{(S + M_S + 1)(S - M_S)}|SM_S + 1\rangle, \\ \hat{S}_-|SM_S\rangle &= \sqrt{(S - M_S + 1)(S + M_S)}|SM_S - 1\rangle, \end{aligned} \tag{31}$$

Alternatively, the matrix representation of $\hat{H}'$ can be constructed by using the basis functions $|JM_J\rangle$, which are linear combinations of the product functions $|LM_L\rangle|SM_S\rangle$. As the electronic structure calculations may already give the energy levels for the orbital states, hereafter we may use $|LM_L\rangle|SM_S\rangle$ as the basis such that the orbital energy of $|LM_L\rangle$ is added only to the diagonal elements. When the ground orbital state is nondegenerate, the diagonalization of the Hamiltonian matrix can be simplified by using the perturbation theory.

Cases of Nondegenerate Orbital States

g-Factor

The g-factor is usually employed to express the ratio between the magnetic moment and the effective spin. For example,

$$\vec{\mu} = \mu_x \hat{x} + \mu_y \hat{y} + \mu_z \hat{z} = -\mu_B (g_x S_x \hat{x} + g_y S_y \hat{y} + g_z S_z \hat{z}), \tag{32}$$

and its interaction with the external field is given by

$$E' = -\vec{\mu} \cdot \vec{H} = \mu_B (g_x S_x H_x + g_y S_y H_y + g_z S_z H_z). \tag{33}$$

According to eq. (28), this energy is equal to

$$E' = \lambda \vec{L} \cdot \vec{S} + \mu_B \vec{L} \cdot \vec{H} + 2\mu_B \vec{S} \cdot \vec{H} \tag{34}$$

For cases when the ground orbital state is nondegenerate, the orbital angular momentum $\vec{L}$ of the above expression can be replaced with eq. (26) so that

$$\begin{aligned} E' = &-2\mu_B \lambda (\Lambda_{xx} S_x H_x + \Lambda_{yy} S_y H_y + \Lambda_{zz} S_z H_z) \\ &- 2\mu_B^2 (\Lambda_{xx} H_x^2 + \Lambda_{yy} H_y^2 + \Lambda_{zz} H_z^2) + 2\mu_B (S_x H_x + S_y H_y + S_z H_z). \end{aligned} \tag{35}$$

The second term with the square of the field may be neglected, because the term $\mu_B H$ is usually much smaller than the spin-orbit coupling energy. Therefore,

$$\begin{aligned} E' \approx &-2\mu_B \lambda (\Lambda_{xx} S_x H_x + \Lambda_{yy} S_y H_y + \Lambda_{zz} S_z H_z) \\ &+ 2\mu_B (S_x H_x + S_y H_y + S_z H_z). \end{aligned} \tag{36}$$

By comparing eq. (33) with eq. (36), we may write

$$g_\mu = 2(1 - \lambda \Lambda_{\mu\mu}) = 2 - 2\lambda \Lambda_{\mu\mu} \qquad (\mu = x, y, z), \tag{37}$$

where $-2\lambda\Lambda_{\mu\mu}$ is the deviation of g from 2. Obviously, such a deviation arises as a consequence of unquenched angular momentum; the greater the unquenched orbital angular momentum, the more the g-factor deviates from 2.

Now let us revisit the example of a Cu^{2+} ion in a field corresponding to a tetragonal D_{4h} symmetry. eq. (27) gives the expressions for the Λ_{xx}, Λ_{yy}, and Λ_{zz}. Thus, by using eq. (37) we can readily obtain

$$g_x = 2 - \frac{2\lambda}{E_2 - E_0}, \tag{38a}$$

$$g_y = 2 - \frac{2\lambda}{E_3 - E_0}, \tag{38b}$$

$$g_z = 2 - \frac{8\lambda}{E_4 - E_0}. \tag{38c}$$

The same results can also be obtained from the unquenched orbital angular momentum of eq. (23). Namely,

$$g_x = \frac{\lambda L_x S_x + 2\mu_B H_x S_x}{\mu_B H_x S_x} = \frac{\lambda L_x}{\mu_B H_x} + 2 = -\frac{\lambda\left(\frac{2\mu_B H_x}{E_2 - E_0}\right)}{\mu_B H_x} + 2$$
$$= 2 - \frac{2\lambda}{E_2 - E_0}.$$
$$g_z = \frac{\lambda L_z S_z + 2\mu_B H_z S_z}{\mu_B H_z S_z} = \frac{\lambda L_z}{\mu_B H_z} + 2 = -\frac{\lambda\left(\frac{8\mu_B H_z}{E_4 - E_0}\right)}{\mu_B H_z} + 2$$
$$= 2 - \frac{8\lambda}{E_4 - E_0}. \quad (39)$$

As a practical example of checking the relative values of g_z and g_x (usually denoted by $g_\parallel$ and $g_\perp$ respectively, in the literature), we consider $Cu(NH_3)_4SO_4{\cdot}H_2O$ for a complex containing a Cu^{2+} ion.[4] We label the spin-orbit coupling constant for the Cu^{2+} ion of $Cu(NH_3)_4SO_4{\cdot}H_2O$ as λ', and that of a free Cu^{2+} ion as λ. Because the d-shell of a Cu^{2+} ion is more than half filled, $\lambda' < 0$ and $\lambda < 0$. In general, for a Cu^{2+} ion located at a Jahn-Teller distorted octahedral site, the local z-axis is taken along the axially elongated direction. Then the xy level is close to the xz and yz levels. As a result, for the Cu^{2+} ion of $Cu(NH_3)_4SO_4{\cdot}H_2O$, eq. (39) can be rewritten as

$$g_z = 2 - \frac{8\lambda'}{\Delta}, \quad (40a)$$

$$g_x = 2 - \frac{2\lambda'}{\Delta}, \quad (40b)$$

where Δ is the energy difference, $\Delta = E(d_{x^2-y^2}) - E(d_{xy})$. Thus the deviation of the g-factor along the z-direction, $\Delta g_z = g_z - 2$, should be greater than that along any direction in the xy-plane direction, $\Delta g_x = g_x - 2$, by a factor of four. This was verified by EPR measurements of $Cu(NH_3)_4SO_4{\cdot}H_2O$, which show that $g_z = 2.22 \pm 0.02$ and $g_x = 2.05 \pm 0.02$.[4] Since the weights of the d-orbitals in the d-block energy levels of $Cu(NH_3)_4SO_4{\cdot}H_2O$ should be less than unity, the λ'/λ ratio should be smaller than unity. From the EPR experiments, $\Delta g_\parallel = 0.22$. Using this result and eq. (40a), the λ'/λ ratio can be written as

$$\frac{\lambda'}{\lambda} = 0.22\left(\frac{\Delta}{8\lambda}\right) \quad (40c)$$

It is found that $\lambda \approx -830\ cm^{-1}$ for a free Cu^{2+} ion (Table 1), and $\Delta \approx 17{,}000\ cm^{-1}$ absorption band lying at 590 nm.[5] Then the λ'/λ ratio is estimated to be approximately 0.55.

The derivation of g-factor from 2 described in eq. (37) is based on the pure classical vector method. A more rigorous derivation requires the construction and the diagonalization of the matrix of the Hamiltonian $\hat{H}'$ given in eq. (28) in terms of the basis functions $|LM_L\rangle|SM_S\rangle$. As already mentioned, such a procedure can be simplified by using the perturbation theory when the ground state is well separated from the excited states.

Effective Spin Approach and g-Factor

In this section we examine the practical use of the g-factor. In general, all the magnetic energy levels of a spin system can be expressed in terms of the spin exchange parameters J. This approach uses only the spin angular momentum $\vec{S}$, so that the low-energy excitations of a magnetic solid are readily described. Therefore, it is convenient to use only the "spin" angular momentum and equate it to the experimentally measured magnetic moment. Nevertheless, the spin-orbit coupling term, i.e., $\lambda\hat{L}\cdot\hat{S}$, contains the orbital angular momentum $\hat{L}$. Furthermore, the Zeeman term $\mu_B(\hat{L} + 2\hat{S})\cdot\vec{H}$ (with $g = 2$) also contains the orbital angular momentum $\hat{L}$. Therefore, it is of interest to remove the orbital angular momentum $\hat{L}$ from the Hamiltonian $\hat{H}'$ in eq. (28) without losing the information about $\hat{L}$. Namely, we wish to discuss the effects of $\hat{H}$ solely in terms of spin basis functions. For this purpose, it is necessary to find the effective Hamiltonian $\hat{H}'_{eff}$ containing only spin operators in which the effects of the orbital angular momentum $\hat{L}$ are absorbed in the g-factor.

In order to find the effective Hamiltonian $\hat{H}'_{eff}$,[6] it is necessary to examine how the Hamiltonian matrix elements of $\hat{H}'$ evaluated in terms of the orbital/spin basis functions $|LM_L\rangle|SM_S\rangle$,

$$\langle S'\ M'_S|\langle L'\ M'_L|\hat{H}'|L\ M_L\rangle|S\ M_S\rangle, \quad (41)$$

can be replaced with the matrix elements of $\hat{H}'_{eff}$ consisting of only spin operators in terms of the spin basis functions $|SM_S\rangle$,

$$\langle S'\ M'_S|\hat{H}'_{eff}|S\ M_S\rangle. \quad (42)$$

When the orbital function $\psi_0 \equiv |LM_L\rangle_G$ for the ground state is nondegenerate, all the integrals $\langle\psi_0|\hat{L}_\mu|\psi_0\rangle = 0$ for $\mu = x, y, z$. Then, the first order perturbation energy correction is given by

$$H^{(1)}_{eff} = \langle\psi_0|\hat{H}'|\psi_0\rangle = 2\mu_B\hat{S}\cdot\vec{H} = 2\mu_B\sum_{\mu=x,y,z}\hat{S}_\mu H_\mu. \quad (43)$$

By noting $\langle\psi_n|\hat{S}|\psi_0\rangle = 0$ when ψ_n and ψ_0 are the excited and ground states, respectively, the second order perturbation energy correction is expressed as

$$H^{(2)}_{eff} = -\sum_n^{\text{excited states}}\frac{|<\psi_0|\lambda\hat{L}\cdot\hat{S} + \mu_B\hat{L}\cdot H|\psi_n>|^2}{E_n - E_0}$$
$$= \sum_{\substack{\mu=x,y,z\\ \upsilon=x,y,z}}[-2\lambda\mu_B H_\mu\Lambda_{\mu\upsilon}\hat{S}_\upsilon - \lambda^2\hat{S}_\mu\Lambda_{\mu\upsilon}\hat{S}_\upsilon - \mu_B^2 H_\mu\Lambda_{\mu\upsilon}H_\upsilon], \quad (44)$$

where

$$\Lambda_{\mu\upsilon} = \sum_n^{\text{excited states}}\frac{<\psi_0|\hat{L}_\mu|\psi_n><\psi_n|\hat{L}_\upsilon|\psi_0>}{E_n - E_0}. \quad (45)$$

Usually $\Lambda_\mu v = 0$ when $\mu \neq v$. Then,

$$\hat{H}'_{eff} = H^{(1)}_{eff} + H^{(2)}_{eff}$$
$$= \sum_{\mu=x,y,z}[2\mu_B\hat{S}_\mu H_\mu - 2\lambda\mu_B H_\mu\Lambda_{\mu\mu}\hat{S}_\mu - \lambda^2\hat{S}_\mu\Lambda_{\mu\upsilon}\hat{S}_\mu - \mu_B^2 H_\mu\Lambda_{\mu\mu}H_\mu]$$
$$= \sum_{\mu=x,y,z}[2(1 - \lambda\Lambda_{\mu\mu})\hat{S}_\mu\mu_B H_\mu - \lambda^2\Lambda_{\mu\mu}\hat{S}^2_\mu - \mu_B^2\Lambda_{\mu\mu}H^2_\mu]. \quad (46a)$$

As already discussed, the third term of the above expression can be neglected so that

$$\begin{aligned}\hat{H}'_{\text{eff}} &= \sum_{\mu=x,y,z} [2(1-\lambda\Lambda_{\mu\mu})\hat{S}_\mu \mu_B H_\mu - \lambda^2 \Lambda_{\mu\mu}\hat{S}^2_\mu] \\ &= \sum_{\mu=x,y,z} [2(1-\lambda\Lambda_{\mu\mu})\hat{S}_\mu \mu_B H_\mu - \lambda^2 \sum_{\mu=x,y,z} \Lambda_{\mu\mu}\hat{S}^2_\mu\end{aligned} \tag{46b}$$

The second term from the above expression does not depend on the external magnetic field. If we were to neglect this term, the effective Hamiltonian $\hat{H}'_{\text{eff}}$ can be expressed only in terms of the spin operators as

$$\hat{H}'_{\text{eff}} = \sum_{\mu=x,y,z} g_\mu \mu_B H_\mu \hat{S}_\mu \tag{46c}$$

where $g_\mu = 2(1 - \lambda\Lambda_{\mu\mu})$. Thus, for nondegenerate cases, the expression of the g-factor obtained from the classical vector approach is the same as that obtained from the perturbation theory. However, it must be noticed that the classical vector approach cannot generate the second term of eq. (46b), which is discussed in the next section.

Zero-Field Splitting

The second term of eq. (46b) is the only term that remains in the effective Hamiltonian $\hat{H}'_{\text{eff}}$ when the external field is zero. Namely, when $\vec{H} = 0$,

$$\hat{H}'_{\text{eff}} = \hat{H}'_{\text{zf}} = -\lambda^2(\Lambda_{xx}\hat{S}^2_x + \Lambda_{yy}\hat{S}^2_y + \Lambda_{zz}\hat{S}^2_z) \tag{47}$$

The zero-field term is usually written in the form of

$$\hat{H}'_{\text{zf}} = D\hat{S}^2_z + E(\hat{S}^2_x - \hat{S}^2_y) - 1/3 D\hat{S}^2, \tag{48}$$

with

$$\begin{aligned} D &= -\lambda^2(-1/2\Lambda_{xx} - 1/2\Lambda_{yy} + \Lambda_{zz}), \\ E &= -1/2\lambda^2(\Lambda_{xx} - \Lambda_{yy}). \end{aligned} \tag{49}$$

It was shown in "Electronic structure and orbital angular momentum" section that the matrix element $\Lambda_{\mu\mu}$ is proportional to the unquenched orbital angular momentum along the μ direction. Therefore, the D parameter represents the difference between the unquenched orbital angular momenta of the parallel (along the z-axis) and perpendicular direction (along the x- or y-axis) directions, namely,

$$D \propto \lambda^2(L_\parallel - L_\perp). \tag{50}$$

Likewise, the E parameter represents the difference between the unquenched orbital angular momenta along the x- and y-directions, i.e.,

$$E \propto \lambda^2(L_x - L_y). \tag{51}$$

In other words, the D and E terms describe a single ion anisotropy caused by the difference between the unquenched orbital angular momenta along three different directions, which originate from the spin-orbit coupling.

To illustrate how the zero-field splitting arises from the single ion anisotropy, we rewrite eq. (48) as

$$\hat{H}'_{\text{zfs}} = D\hat{S}^2_z + 1/2 E(\hat{S}_+\hat{S}_+ + \hat{S}_-\hat{S}_-) - 1/3 D\hat{S}^2 \equiv \hat{H}_{\text{sia}} - 1/3 D\hat{S}^2 \tag{52}$$

and consider two simple examples:

1. Case of $S = 1/2$:
   A doublet state is described by two spin functions,

   $$\phi_1 = |1/2 + 1/2\rangle = |\uparrow\rangle, \qquad \phi_2 = |1/2 - 1/2\rangle = |\downarrow\rangle.$$

   In terms of these functions it is straightforward to find the matrix elements

   $$(\mathbf{H}_{\text{sia}})_{11} = \langle\phi_1|\hat{H}_{\text{sia}}|\phi_1\rangle = +D/4. \quad (\mathbf{H}_{\text{sia}})_{12} = \langle\phi_1|\hat{H}_{\text{sia}}|\phi_2\rangle = 0,$$

   $$(\mathbf{H}_{\text{sia}})_{21} = \langle\phi_2|\hat{H}_{\text{sia}}|\phi_1\rangle = 0, \quad (\mathbf{H}_{\text{sia}})_{22} = \langle\phi_2|\hat{H}_{\text{sia}}|\phi_2\rangle = +D/4.$$

   Thus the 2×2 matrix representation of the anisotropic Hamiltonian $\hat{H}_{\text{sia}}$ is given by

   $$\mathbf{H}_{\text{sia}} = +(D/4)\begin{pmatrix} 1 & 0 \\ 0 & 1 \end{pmatrix}. \tag{53}$$

   Since the functions ϕ_1 and ϕ_2 do not interact under the Hamiltonian $\hat{H}_{\text{sia}}$, the two spin states should remain degenerate at energy $+D/4$. The isotropic term $-(D/3)\hat{S}^2$ of $\hat{H}_{\text{zfs}}$ leads to the energy,

   $$-(D/3)\hat{S}^2 \longrightarrow -(D/3)S(S+1) = -(D/3)(1/2)(3/2) = -D/4. \tag{54}$$

   The sum of the isotropic energy $-D/4$ and the anisotropic energy $+D/4$ is zero, so the energy levels remain unchanged. In other words, a doublet spin state does not exhibit single ion anisotropy.
2. Case of $S = 1$:
   A triplet state is described by three spin functions,

   $$\phi_1 = |1\ 1\rangle = |\uparrow\uparrow\rangle,$$

   $$\phi_2 = |1\ 0\rangle = \sqrt{1/2}\,(|\uparrow\downarrow\rangle + |\uparrow\downarrow\rangle),$$

   $$\phi_3 = |1\ -1\rangle = |\uparrow\downarrow\rangle.$$

   Then, we find

   $$\hat{H}_{\text{sia}}|\phi_1\rangle = D|\phi_1\rangle + E|\phi_3\rangle,$$

   $$\hat{H}_{\text{sia}}|\phi_2\rangle = 0,$$

   $$\hat{H}_{\text{sia}}|\phi_3\rangle = D|\phi_3\rangle + E|\phi_1\rangle.$$

Therefore,

$$(\mathbf{H}_{\rm sia})_{11}\langle\phi_1|\hat{H}_{\rm sia}|\phi_1\rangle = D, \quad (\mathbf{H}_{\rm sia})_{12}\langle|\phi_1|\hat{H}_{\rm sia}|\phi_2\rangle = 0,$$
$$(\mathbf{H}_{\rm sia})_{13}\langle\phi_1|\hat{H}_{\rm sia}|\phi_3\rangle = E, \quad (\mathbf{H}_{\rm sia})_{22}\langle\phi_2|\hat{H}_{\rm sia}|\phi_2\rangle = 0,$$
$$(\mathbf{H}_{\rm sia})_{23}|\phi_2|\hat{H}_{\rm sia}|\phi_3\rangle = 0, \quad (\mathbf{H}_{\rm sia})_{33}\langle\phi_3|\hat{H}_{\rm sia}|\phi_3\rangle = D.$$

Thus the 3 × 3 matrix representation of the anisotropic Hamiltonian $\hat{H}_{\rm sia}$ is given by

$$\mathbf{H}_{\rm sia} = \begin{pmatrix} D & 0 & E \\ 0 & 0 & 0 \\ E & 0 & D \end{pmatrix}. \tag{55}$$

Note that the functions $\phi_1 = |\uparrow\uparrow\rangle$ and $\phi_3 = |\downarrow\downarrow\rangle$ interact under the anisotropic Hamiltonian $\hat{H}_{\rm sia}$. The diagonalization of the matrix $\mathbf{H}_{\rm sia}$ generates the eigenvalues and eigenfunctions as

$$E_0 = 0, \quad \psi_0 = \phi_2 = \sqrt{1/2}(|\uparrow\downarrow\rangle + |\downarrow\uparrow\rangle),$$
$$E_+ = D + E, \quad \psi_+ = \sqrt{1/2}(\phi_1 + \phi_3) = \sqrt{1/2}(|\uparrow\uparrow\rangle + |\downarrow\downarrow\rangle),$$
$$E_- = D - E, \quad \psi_- = \sqrt{1/2}(\phi_1 + \phi_3) = \sqrt{1/2}(|\uparrow\uparrow\rangle + |\downarrow\downarrow\rangle). \tag{56}$$

The isotropic term $-{}^1\!/_3 D\hat{S}^2$ leads to the energy,

$$-{}^1\!/_3 D\hat{S}^2 \longrightarrow -{}^1\!/_3 DS(S+1) = -{}^1\!/_3 D \times 1 \times 2 = -{}^2\!/_3 D.$$

Therefore, the energies of the Hamiltonian $\hat{H}'_{\rm eff}$ become

$$E_0 = -{}^2\!/_3 D,$$
$$E_+ = {}^1\!/_3 D + E, \tag{57}$$
$$E_- = {}^1\!/_3 D - E.$$

Cases of Degenerate Orbital States

When the ground states are degenerate, the g-factor cannot be calculated by employing either the classical vector method or the nondegenerate perturbation theory discussed in the previous section. For such systems, it is necessary to construct the matrix representation of the Hamiltonian $\hat{H}' = \lambda\hat{L}\cdot\hat{S} + \mu_B(\hat{L} + 2\hat{S})\cdot\vec{H}$, eq. (28), in terms of the basis $|LM_{\rm L}\rangle|SM_{\rm S}\rangle$, add the energy of the orbital state $|LM_{\rm L}\rangle$ to the diagonal elements, and diagonalize the resulting matrix. This gives rise to the eigenvalues and eigenfunctions, from which the g-factor can be calculated. In general, the energy splitting induced by a crystal field and a spin-orbit coupling is of the order of 10^{-2} to 10^{-1} eV, while that induced by an external magnetic field is much smaller (e.g., $\mu_{\rm B}H \approx 5.8 \times 10^{-5}$ eV at $H = 1$ T). Therefore, the Zeeman term $\mu_B(\hat{L} + 2\hat{S})\cdot\vec{H}$ can be treated as a perturbation. Namely, one may first obtain the eigenstates for the Hamiltonian $\hat{H}_{\rm CF} + \hat{H}_{\rm SO}$ consisting of the crystal field and spin-orbit terms, and then use the resulting eigenfunctions to calculate the expectation values of the Zeeman Hamiltonian $\hat{H}_{\rm Z}$ by using the degenerate perturbation theory and consequently calculate the g-factor. Let us explore this approach by considering two examples, as discussed below.

High-Spin d^7 Ions at Octahedral Sites

First, let us discuss the magnetic anisotropy of $CoCl_2$ described by Lines.[7] The building blocks of $CoCl_2$ are layers of composition $CoCl_2$ that are made up of edge-sharing $CoCl_6$ octahedra (Fig. 2). Each Co^{2+} (d^7) ion, located at the center of a $CoCl_6$ octahedron, is in the high-spin state. Thus the local d-block electronic structure of each Co^{2+} ion is described by the electron configuration $(t_{2g})^5(e_g)^2$ with three unpaired spins. Each $CoCl_6$ octahedron is weakly distorted to become trigonal in symmetry, namely, it is slightly flattened along the threefold rotational axis that is perpendicular to the $CoCl_2$ layer (Fig. 2a). To a first approximation, each Co^{2+} ion of $CoCl_2$ is in a cubic crystal field due to its octahedral coordination. The weak distortion of each $CoCl_6$ octahedron adds a weak trigonal crystal field to each Co^{2+} ion. The magnetic anisotropy of $CoCl_2$ at low temperatures is primarily determined by the ground orbital state of each Co^{2+} ion.

The ground orbital state of a free Co^{2+} (d^7) ion is ^{4}F (i.e., $L = 3$, $S = 3/2$). In a cubic crystal field this state is split into $^4A_2$, $^4T_2$, and $^4T_1$ states. Of the three states, the ground orbital state is the orbital triplet state $^4T_1$, which is described by[7]

$$\phi_{+1} = \sqrt{{}^5\!/_6}|3\ -2\rangle - \sqrt{{}^1\!/_6}|3\ 1\rangle$$
$$\phi_0 = {}^2\!/_3|3\ 0\rangle - {}^1\!/_3\sqrt{{}^5\!/_2}(|3\ 3\rangle - |3\ -3\rangle), \tag{58}$$
$$\phi_{-1} = \sqrt{{}^5\!/_6}|3\ 2\rangle + \sqrt{{}^1\!/_6}|3\ -1\rangle$$

where the orbital momentum states $|LM_{\rm L}\rangle$ refer to those of a free ion. In terms of the momentum operator $\hat{L}_z$ of a free ion, it can be easily shown by using eq. (16) that

$$\langle\phi_{+1}|\hat{L}_z|\phi_{+1}\rangle = -3/2,$$
$$\langle\phi_0|\hat{L}_z|\phi_0\rangle = 0, \tag{59}$$
$$\langle\phi_{-1}|\hat{L}_z|\phi_{-1}\rangle = 3/2.$$

In addition, all the matrix elements of $\hat{H}$ between the three states ϕ_{+1}, ϕ_0, and ϕ_{-1} are exactly the same as those of $-{}^3\!/_2\hat{L}$ between the corresponding P states of a free ion (i.e., $L = 1$, $M_{\rm L} = 1, 0, -1$). Therefore, as far as the orbital triplet state $^4T_1$ is concerned, the orbital momentum of a Co^{2+} ion in a cubic crystal field can be discussed by using the pseudo-orbital momentum operator $-{}^3\!/_2\hat{L}$ with the effective orbital states $|L'M_{L'}\rangle$, where $L' = 1$ and $M_{L'} = 1, 0, -1$ as if the Co^{2+} ion is a free ion. Then, the orbital/spin states of $^4T_1$ can be represented by $|L'M_{L'}\rangle|SM_{\rm S}\rangle$. Here $S = 3/2$ so that $M_{\rm S} = 3/2, 1/2, -1/2, -3/2$. Because the values of L' and S are fixed, the notations $|L'M_{L'}\rangle|SM_{\rm S}\rangle$ can be simplified as $|M_{L'}M_{\rm S}\rangle$. Consequently, the ground orbital triplet state $^4T_1$ of a Co^{2+} (d^7) ion in a cubic field is described by 12 $|M_{L'}M_{\rm S}\rangle$ functions ($M_{L'} = 1, 0, -1$; $M_{\rm S} = 3/2, 1/2, -1/2, -3/2$).

As mentioned above, each Co^{2+} ion of $CoCl_2$ is under a weak trigonal crystal field due to the slight trigonal distortion of

each $CoCl_6$ octahedron. This distortion and the spin-orbit coupling will split the 12 $|M_{L'}M_S\rangle$ states of each Co^{2+} ion. To find the ground state of these split levels, we first note that in a trigonal crystal field the orbital triplet is split into an orbital doublet and an orbital singlet with energy separation δ. This can be described by the phenomenological Hamiltonian $\hat{H}_{CF}$ defined by

$$\hat{H}_{CF} = -\delta(\hat{L}_z^2 - \tfrac{2}{3}), \tag{60}$$

which places the states $|1M_S\rangle$ and $|-1M_S\rangle$ at $-1/3\delta$, and the state $|0M_S\rangle$ at $2/3\delta$. In describing the spin-orbit coupling of a Co^{2+} ion in a trigonal distortion in terms of $\hat{H}_{SO}$, the pure orbital momentum operator $\hat{L}$ is replaced with the pseudo-orbital operator $-3/2k\hat{L}$. Here the constant k is the "orbital reduction factor" (slightly smaller than unity), which is included to reflect the fact that a Co^{2+} ion of $CoCl_2$ has a smaller angular momentum (in magnitude) than does a free Co^{2+} ion because the 3d orbitals of a Co^{2+} ion in the magnetic orbitals of $CoCl_2$ have a weight smaller than unity. Thus the Hamiltonian $\hat{H}_{SO}$ is modified as

$$\hat{H}_{SO} = -3/2k\lambda\hat{L}\cdot\hat{S} \tag{61}$$

Then, the combined Hamiltonian $\hat{H}' = \hat{H}_{CF} + \hat{H}_{SO}$ can be regarded as perturbation to find how the 12 $|M_{L'}M_S\rangle$ states of $^4T_1$ are split by the trigonal distortion and the spin-orbit interaction.

$$\begin{aligned}\hat{H}' &= -\delta(\hat{L}_z^2 - \tfrac{2}{3}) - \tfrac{3}{2}k\lambda\hat{L}\cdot\hat{S} \\ &= -\delta(\hat{L}_z^2 - \tfrac{2}{3}) - \tfrac{3}{2}k\lambda\left[\hat{L}_z\hat{S}_z + \tfrac{1}{2}(\hat{L}_+\hat{S}_- + \hat{L}_+\hat{S}_-)\right]\end{aligned} \tag{62}$$

The matrix elements of $\hat{H}'$ for $|M_{L'}M_S\rangle$ are found to be the same as those for $|-M_{L'} - M_S\rangle$, that is, the 12 $|M_{L'}M_S\rangle$ states are split into six spin doublets (i.e., six Kramers' doublets). Furthermore, calculations of the eigenvalues of $\hat{H}'$ as a function of the $\delta/k\lambda$ ratio reveal that the ground Kramers' doublet state is described by the two functions[7]

$$\begin{aligned}\psi_+ &= c_1\left|-1\ \tfrac{3}{2}\right\rangle + c_2\left|0\ \tfrac{1}{2}\right\rangle + c_3\left|1\ -\tfrac{1}{2}\right\rangle \\ \psi_- &= c_1\left|1\ -\tfrac{3}{2}\right\rangle + c_2\left|0\ -\tfrac{1}{2}\right\rangle + c_3\left|-1\ \tfrac{1}{2}\right\rangle\end{aligned} \tag{63}$$

where the coefficients c_1, c_2, and c_3 are determined by the $\delta/(k\lambda)$ value applicable to $CoCl_2$.[7]

Suppose that an external field $H_\parallel$ is applied parallel to the trigonal axis (i.e., the local z-axis), so the corresponding Zeeman Hamiltonian becomes

$$\hat{H}_{Z\parallel} = (-3/2k\hat{L}_z + 2\hat{S}_z)\mu_B H_\parallel. \tag{64}$$

This Hamiltonian splits the degeneracy of the ground doublet state and introduces a energy gap of $\Delta E_\parallel$ between ψ_+ and ψ_-. According to the first order degenerate perturbation theory, $\Delta E_\parallel$ is expressed as

$$\Delta E_\parallel = \left|\langle\psi_+|\hat{H}_{z\parallel}|\psi_+\rangle - \langle\psi_-|\hat{H}_{z\parallel}|\psi_-\rangle\right|. \tag{65}$$

Consequently, the g-factor for the parallel direction, $g_\parallel$, is obtained as

$$g_\parallel = \frac{\Delta E_\parallel}{\mu_B H_\parallel} = (6+3k)c_1^2 + 2c_2^2 - (3k+2)c_3^2. \tag{66}$$

Suppose now that an external magnetic field is perpendicular to the trigonal axis (e.g., the local x-axis) with the strength $H_\perp$, so the corresponding Zeeman Hamiltonian becomes

$$\begin{aligned}\hat{H}_{Z\perp} &= (-3/2k\hat{L}_x + 2\hat{S}_x)\mu_B H_\perp \\ &= [-3/4k(\hat{L}_+ + \hat{L}_-) + (\hat{S}_+ + \hat{S}_-)]\mu_B H_\perp.\end{aligned} \tag{67}$$

According to the first order degenerate perturbation theory, the energy split $\Delta E_\perp$ of the ground doublet state caused by $\hat{H}_{Z\perp}$ is expressed as

$$\Delta E_\perp = \left|\langle\psi_+|\hat{H}_{Z\perp}|\psi_+\rangle - \langle\psi_-|\hat{H}_{Z\perp}|\psi_-\rangle\right|. \tag{68}$$

Thus, the g-factor for the perpendicular direction, $g_\perp$, is obtained as

$$g_\perp = \frac{\Delta E_\perp}{\mu_B H_\perp} = 4c_2^2 + 4\sqrt{3}c_1c_3 - 3\sqrt{2}kc_2c_3. \tag{69}$$

High-Spin d^6 Ions at Trigonal Prism and Linear Two Coordinate Sites

A hexagonal perovskite-type oxide $Ca_3Co_2O_6$ consists of $(Co_2O_6)_\infty$ chains separated by Ca atoms, and each $(Co_2O_6)_\infty$ chain has CoO_6 octahedra alternating with CoO_6 trigonal prisms[3] by sharing their triangular faces (Fig. 3).[8] The magnetic properties of $Ca_3Co_2O_6$ are uniaxial[9–11] and are described by an Ising spin Hamiltonian. Recent experimental[12,13] and theoretical studies (Zhang et al., unpublished)[14] established that each octahedral-site cobalt is essentially nonmagnetic with a low-spin Co^{3+} (d^6) ion, and each trigonal prism-cobalt has a high-spin Co^{3+} (d^6) ion with four unpaired spins ($S = 2$). Consequently, the highly anisotropic magnetic properties of $Ca_3Co_2O_6$ are associated with the high-spin d^6 ions at the trigonal prism sites. This implies that the magnetic moment of a high-spin d^6 ion at each trigonal prism site is parallel to its threefold rotational axis. Hereafter, the directions parallel and perpendicular to the n-fold rotational axis of a coordination site with $n \geq 3$ will be referred to as the parallel and perpendicular directions, respectively. Thus, the magnetic moment is nonzero along the parallel direction ($\mu_\parallel = 4.8\ \mu_B$)[11] and zero along the perpendicular direction ($\mu_\perp = 0$).

In the high-spin Fe^{2+} (d^6) complex $Fe[C(SiMe_3)_3]_2$,[15] linear two-coordinate Fe^{2+} ions are located at sites with D_{3d} symmetry. The Mössbauer study of $Fe[C(SiMe_3)_3]_2$[16] showed that the contribution of the orbital moment to the internal field is equivalent to adding two full spins relative to spin only $S = 2$ behavior. Furthermore, the analysis of the electric field gradient tensor and the direction of the internal hyperfine fields showed that the magnetic properties of $Fe[C(SiMe_3)_3]_2$ are uniaxial.

The 3d orbitals of a high-spin Co^{3+} (d^6) ion at a CoO_6 trigonal prism are split as shown in Figure 4a, and those of a high-spin Fe^{2+} (d^6) at a linear $Fe[C(SiMe_3)_3]_2$ unit as shown in Figure 4b, where the local z-axis is taken along the threefold

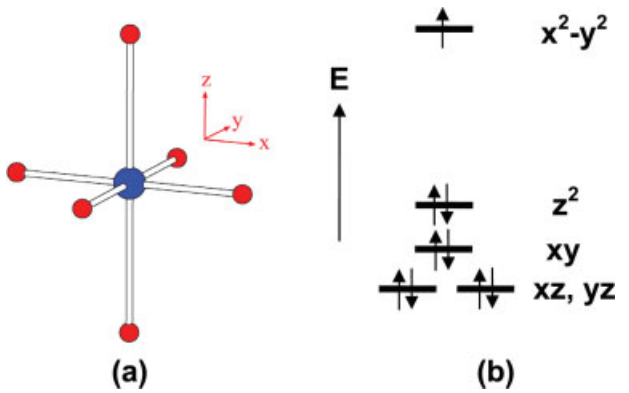

Figure 1. (a) An axially elongated CuL_6 octahedron containing Cu^{2+} (d^9) ion and (b) the relative ordering of its d-block energy levels.

rotational axis. The Cartesian forms of the d orbitals correspond to the orbital angular momentum states $|LM_L\rangle$ ($L = 2$, $M_L = -2, 1, 0, 1, 2$) as indicated below.

$$\begin{array}{lcl} \{z^2\} & \leftrightarrow & \{|2\ 0\rangle\} \\ \{x^2 - y^2, xy\} & \leftrightarrow & \{|2\ -2\rangle,\ |2\ 2\rangle\} \\ \{xz, yz\} & \leftrightarrow & \{|2\ -1\rangle,\ |2\ 1\rangle\} \end{array} \quad (70)$$

For our discussion, it is important to recognize the low-energy electron configurations for high-spin d^6 ions at trigonal prism and linear two-coordinate sites. Figure 5 shows three low-energy electron configurations of a high-spin Co^{3+} (d^6) ion at a trigonal prism site, where the orbitals are labeled in terms of their M_L values. $L = 0$ for the nondegenerate configuration (Fig. 5a), while $L = 2$ for the two degenerate configurations (Figs. 5b and 5c). The nondegenerate configuration ($L = 0$) does not contribute to spin-orbit coupling, but the two degenerate configurations ($L \neq 0$) do. For a high-spin Fe^{2+} (d^6) at a linear two-coordinate site, the ground electronic state should be expressed as linear combinations of two degenerate electron configurations (Fig. 6), for which $L = 2$. Under the effect of crystal field and spin-orbit coupling, doubly degenerate electron configurations of high-spin

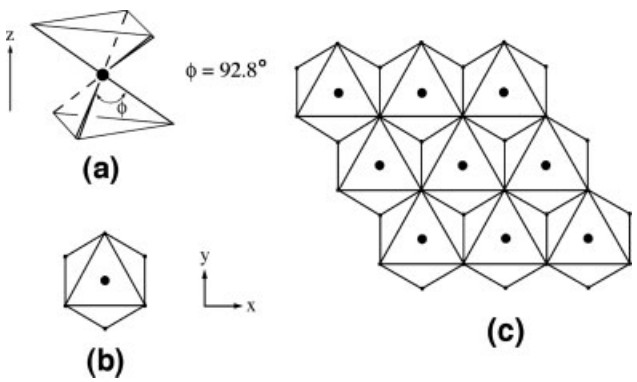

Figure 2. (a) Ball and stick view of a CoO_6 octahedron. (b) Polyhederal representation of a CoO_6 octahedron. (c) Polyhedral representation of an isolated CoO_2 layer made up of edge-sharing CoO_6 octahedra.

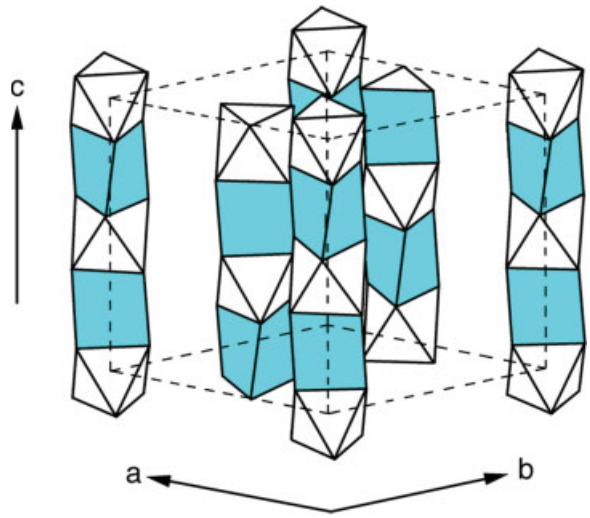

Figure 3. Perspective view of the Co_2O_6 chains of $Ca_3Co_2O_6$. In each Co_2O_6 chain the CoO_6 octahedra and the CoO_6 trigonal prisms are indicated by the absence and the presence of shading, respectively. For simplicity, the Ca^{2+} ions present between the Co_2O_6 chains are not shown.

d^6 ions at trigonal prism and linear two-coordinate sites give rise to doublet states, which are crucial in determining the anisotropy of magnetic properties (see below).

Under the trigonal prism or linear crystal field, the basis function $|LM_L\rangle$ is an eigenfunction of the crystal field Hamiltonian $\hat{H}_{CF}$,[3] so that M_L is still a good quantum number for these crystal fields. As a consequence, the matrix representation of $\hat{H}_{CF} + \hat{H}_{SO}$ using the functions $|LM_L\rangle|SM_S\rangle$ as basis functions is block-diagonalized in terms of $M_J = M_L + M_S$. Since $L = 2$ and $S = 2$ for the ^5D state, there are nine such blocks classified by $M_J = 0$, ±1, ±2, ±3, and ±4. Using the simplified notations $|M_L M_S\rangle \equiv |LM_L\rangle|SM_S\rangle$, the matrix elements

$$\langle M_L\ M_S|\hat{H}_{CF} + \hat{H}_{SO}|M'_L M'_S\rangle$$

are summarized in Table 4. By diagonalizing these blocks, the eigenfunctions $\hat{H}_{CF} + \hat{H}_{SO}$ can be written as

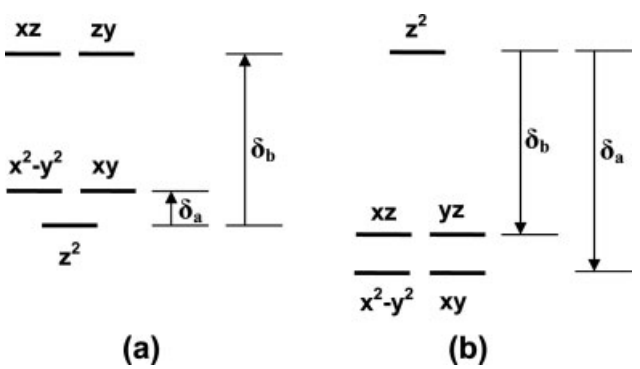

Figure 4. (a) Split pattern of the d-block levels of a transition metal cation at a trigonal prism site. (b) Split pattern of the d-block levels of a transition metal cation at a linear two-coordinate site.

$$
\begin{aligned}
M_J = 0 &: \Phi_0 = a_1(|+2\,-2\rangle + |-2\,+2\rangle) + a_2(|+1\,-1\rangle + |-1\,+1\rangle) + a_3|0\,0\rangle,\\
M_J = \pm 1 &: \Phi_{+1} = b_1|+2\,-1\rangle + b_2|+1\,0\rangle + b_3|0\,+1\rangle + b_4|-1\,+2\rangle,\\
&\quad\ \Phi_{-1} = b_1|-2\,+1\rangle + b_2|-1\,0\rangle + b_3|0\,-1\rangle + b_4|+1\,-2\rangle,\\
M_J = \pm 2 &: \Phi_{+2} = c_1|+2\,0\rangle + c_2|+1\,+1\rangle + c_3|0\,+2\rangle,\\
&\quad\ \Phi_{-2} = c_1|-2\,0\rangle + c_2|-1\,-1\rangle + c_3|0\,-2\rangle,\\
M_J = \pm 3 &: \Phi_{+3} = d_1|+2\,+1\rangle + d_2|+1\,+2\rangle,\\
&\quad\ \Phi_{-3} = d_1|-2\,-1\rangle + d_2|-1\,-2\rangle,\\
M_J = \pm 4 &: \Phi_{+4} = |+2\,+2\rangle,\\
&\quad\ \Phi_{-4} = |-2\,-2\rangle,
\end{aligned}
\tag{71}
$$

where a_i, b_i, c_i, and d_i (i = 1, 2, 3, 4) are coefficients that depend on the three parameters δ_a, δ_b, and λ, where

$$\delta_a = E(M_L = \pm 2) - E(M_L = 0),$$
$$\delta_b = E(M_L = \pm 1) - E(M_L = 0),$$

as shown in Figure 4. The state Φ_0 is a singlet, and the states $\Phi_{\pm n}$ (n = 1–4) are doublets. The eigenvalues E_0 and $E_{\pm n}$ (n = 1–4) associated with these eigenstates also depend on the three parameters δ_a, δ_b, and λ. For numerical calculations, it is convenient to express the state energies E_i (i = 0, ± n) and one crystal field parameter (e.g., δ_b) in units of $|\lambda|$. Then, for a certain δ_a/δ_b ratio appropriate for a given crystal field, the energies $E_i/|\lambda|$ can be readily calculated and plotted as a function of $\delta_b/|\lambda|$. Results of our calculations for a representative case (i.e., $\delta_a/\delta_b = 0.2$ and $\delta_b > 0$) are summarized in Figure 7a. The crystal field Hamiltonian for a linear two-coordinate system has the same expression as does that for a trigonal prism. Therefore, our description for a trigonal prism is also valid for a linear two-coordinate system. The only difference between the two lies in the ranges of the parameters δ_a, δ_b, and λ. Results of our calculations for a representative linear system (i.e., $\delta_a/\delta_b = 1.2$ and $\delta_b < 0$) are summarized in Figure 8a.

The eigenstates of a high-spin d^6 ion at a trigonal prism or a linear two-coordinate site under the zero-field Hamiltonian $\hat{H}_{CF} + \hat{H}_{SO}$ are either a singlet Φ_0 with $M_J = 0$ or a doublet $\Phi_{\pm n}$ with $M_J = \pm n$. For the singlet Φ_0, the Zeeman operator $\hat{H}_Z$ does not induce any splitting so that $g_\parallel = g_\perp = 0$. Each doublet state, described by two functions Φ_{+n} and Φ_{-n}, is doubly degenerate so that the energy split, ΔE_n, between the two under the action of $\hat{H}_Z$ can be determined by employing first-order perturbation theory.[3] When the field is applied along the parallel direction,

$$g_{n\parallel} = \Delta E_{n\parallel}/\mu_B H_\parallel = \langle \Phi_{+n}|\hat{L}_z + 2\hat{S}_z|\Phi_{+n}\rangle = \langle \Phi_{-n}|\hat{L}_z + 2\hat{S}_z|\Phi_{-n}\rangle. \tag{72}$$

When the field is along the perpendicular direction,

$$g_{n\perp} = \Delta E_{n\perp}/\mu_B H_\perp = \langle \Phi_{+n}|(\hat{L}_+ + \hat{L}_-) + 2(\hat{S}_+ + \hat{S}_-)|\Phi_{-n}\rangle. \tag{73}$$

By combining eqs. (72) and (73) with eq. (71), we obtain the following results:

$$
\begin{aligned}
M_J = \pm 1: &\quad g_{1\parallel} = 2b_2^2 + 4b_3^2 + 6b_4^2,\\
M_J = \pm 2: &\quad g_{2\parallel} = 4c_1^2 + 6c_2^2 + 8c_3^2,\\
M_J = \pm 3: &\quad g_{3\parallel} = 8d_1^2 + 10d_2^2,\\
M_J = \pm 4: &\quad g_{4\parallel} = 12.
\end{aligned}
\tag{74}
$$

and

$$g_{n\perp} = 0 \quad \text{for } n = 1, 2, 3, 4. \tag{75}$$

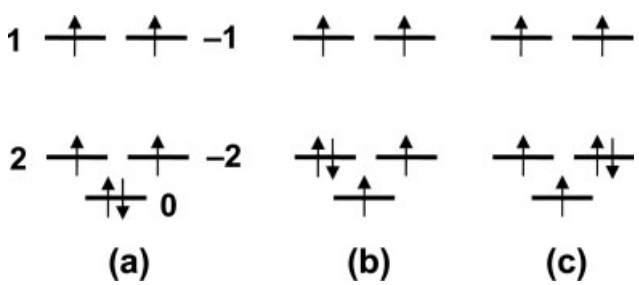

Figure 5. Three low-energy electron configurations of a high-spin d^6 ion at a trigonal prism site.

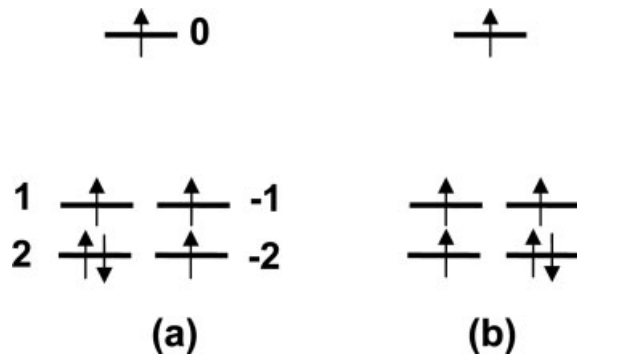

Figure 6. Two degenerate electron configurations of a high-spin d^6 ion at a linear two-coordinate site.

Table 4. Matrix Elements of the Hamiltonian $\hat{H}_{CF} + \hat{H}_{SO}$ for a Transition Metal Ion Located at a Trigonal Prism Site in Terms of the Basis Functions $|L_z\ S_z\rangle \equiv |2\ L_z\rangle|2\ S_z\rangle$.

	$\|2\ -2\rangle$	$\|1\ -1\rangle$	$\|0\ 0\rangle$	$\|-1\ 1\rangle$	$\|-2\ 2\rangle$
$J_z = 0$ block					
$\|2\ -2\rangle$	$\delta_a - 4\lambda$	2λ	0	0	0
$\|1\ -1\rangle$	2λ	$\delta_b - \lambda$	3λ	0	0
$\|0\ 0\rangle$	0	3λ	0	3λ	0
$\|-1\ 1\rangle$	0	0	3λ	$\delta_b - \lambda$	2λ
$\|-2\ 2\rangle$	0	0	0	2λ	$\delta_a - 4\lambda$
	$'2\ -1\rangle$	$\|1\ 0\rangle$	$\|0\ 1\rangle$	$\|-1\ 2\rangle$	
$J_z = 1$ block[a]					
$\|2\ -1\rangle$	$\delta_a - 2\lambda$	$\sqrt{6}\lambda$	0	$\|0$	
$\|1\ 0\rangle$	$\sqrt{6}$	δ_b	3λ	0	
$\|0\ 1\rangle$	0	3λ	0	$\sqrt{6}$	
$\|-1\ 2\rangle$	0	0	$\sqrt{6}\lambda$	$\delta_b - 2\lambda$	
	$'2\ 0\rangle$	$\|1\ 1\rangle$	$\|0\ 2\rangle$		
$J_z = 2$ block[a]					
$\|2\ 0\rangle$	δ_a	$\sqrt{6}\lambda$	0		
$\|1\ 1\rangle$	$\sqrt{6}\lambda$	$\delta_b + \lambda$	$\sqrt{6}\lambda$		
$\|0\ 2\rangle$	0	$\sqrt{6}\lambda$	0		
	$\|2\ 1\rangle$	$\|1\ 2\rangle$			
$J_z = 3$ block[a]					
$\|2\ 1\rangle$	$\delta_a + 2\lambda$	2λ			
$\|1\ 2\rangle$	2λ	$\delta_b + 2\lambda$			
	$\|2\ 2\rangle$				
$J_z = 4$ block[a]					
$\|2\ 2\rangle$	$\delta_a + 4\lambda$				

[a]The elements for the $J_z = -1$, -2, -3, and -4 blocks are the same as those for the $J_z = 1$, 2, 3, and 4 blocks, respectively, except for the basis change from $|L_z\ S_z\rangle$ to $|-L_z\ -S_z\rangle$.

In general, $g_{n\parallel} \neq 0$ (see Figs. 7b and 8b) while $g_{n\perp} = 0$, so a high-spin d^6 ion at a trigonal prism or a linear two-coordinate site show uniaxial magnetic property. The key to explain the uniaxial property is to understand the reason for $g_{n\perp} = 0$. The M_J value for each doublet state $\Phi_{\pm n}$ is given by $\pm n$, where n is an integer greater than zero. Therefore, the M_J value for each basis function of Φ_{+n} is greater than that for each basis function of Φ_{-n} by $2n$ (= 2, 4, 6, etc). However, for each basis function of Φ_{-n}, the operators $\hat{L}_+$ and $\hat{S}_+$ change its M_J value by + 1, while the operators $\hat{L}_-$ and $\hat{S}_-$ change it by -1. Consequently, the integral $\langle\Phi_{+n}|(\hat{L}_+ + \hat{L}_-) + 2(\hat{S}_+ + \hat{S}_-)|\Phi_{-n}\rangle$ vanishes, so that $g_{n\perp} = 0$, which gives rise to uniaxial magnetic property for compounds containing a high-spin d^6 ion at a trigonal prism or a linear two-coordinate site. In principle, the eigenstates of the zero-field Hamiltonian, $\hat{H}_{CF} + \hat{H}_{SO}$, can interact under the Zeeman Hamiltonian

$$\hat{H}_{Z\perp} = \mu_B H_\perp \left[(\hat{L}_+ + \hat{L}_-) + 2(\hat{S}_+ + \hat{S}_-)\right]/2, \qquad (76)$$

if their M_J values differ by 1 (i.e., $\Delta M_J = 1$), e.g., Φ_0 and $\Phi_{\pm 1}$, $\Phi_{\pm 1}$, and $\Phi_{\pm 2}$, and so on. Such interactions give rise to second-order perturbation energy corrections. In general, however, the energy separation between such pairs of zero-field eigenstates is much larger than the maximum available magnetic energy $\mu_B H_{max}$ in a given experiment (i.e., magnetization, EPR or magnetic susceptibility measurements). Therefore, the associated second-order energy corrections are negligible, and so is their effect on the perpendicular g-factor, $g_\perp$.

For a high-spin d^6 ion at a trigonal prism site, a large $\delta_b/|\lambda|$ value is appropriate. Thus, Figure 7a shows that the magnetic ground state is a singlet ($M_J = 0$), the first excited state is a doublet $\Phi_{\pm 1}$ with $M_J = \pm 1$, and the second excited state is a doublet $\Phi_{\pm 2}$ with $M_J = \pm 2$. With increasing the $\delta_b/|\lambda|$ value, the first excited state becomes almost degenerate with the ground state while the second excited states becomes close to the first excited state. As shown in Figure 7b, the singlet ground state contributes zero to $g_\parallel$, the first excited state contributes 4 to $g_\parallel$, and the second excited state contributes 8 to $g_\parallel$. Thus, the parallel magnetic moment $\mu_\parallel = g_\parallel |M_J| \mu_B$ is zero from the singlet Φ_0, $4\mu_B$ from the doublet $\Phi_{\pm 1}$, and $16\mu_B$ from the doublet $\Phi_{\pm 2}$. For $Ca_3Co_2O_6$ whose CoO_6 trigonal prism sites contain high-spin Co^{3+} (d^6) ions, Maignan et al. obtained $\mu_\parallel = 4.8\mu_B$ at 2 K when $H > 8$ T.[11] To explain $\mu_\parallel = 4.8\mu_B$ at 2 K, the singlet state Φ_0 cannot be the ground state, and the doublet state $\Phi_{\pm 1}$ should be the ground state. Indeed, this situation arises for $Ca_3Co_2O_6$ when the spins of the high-spin Co^{3+} ions at the trigonal prism sites adopt a ferromagnetic spin arrangement in each Co_2O_6 chain. For further discussion, see "Uniaxial magnetism as a consequence of electron correlation, direct metal–metal bonding, ferromagnetism, and spin-orbit coupling" section.

For a high-spin d^6 ion at a linear two-coordinate site, a large negative $\delta_b/|\lambda|$ value is appropriate. Figure 8a shows that the magnetic ground state is a doublet with $M_J = \pm 4$, the first excited state is a doublet with $M_J = \pm 3$, and the second excited state is a doublet with $M_J = \pm 2$, and so on. As the $\delta_b/|\lambda|$ value becomes more strongly negative, the energy differences between the ground state and the excited states become larger. Then the magnetic properties of a high-spin d^6 ion at a linear two-coordinate site should be governed by the ground state. This conclusion is supported by the uniaxial magnetic properties of $Fe[C(SiMe_3)_3]_2$.[16] Figure 8b shows that the $g_\parallel$ value of the ground state (i.e., the doublet with $M_J = \pm 4$) is 12. Our findings for a high-spin d^6 ion in a linear two-coordinate system (i.e., $M_J = \pm 4$, $g_\parallel = 12$, and $g_\perp = 0$ for the ground state) are consistent with the experimental observations for $Fe[C(SiMe_3)_3]_2$.[16]

Simple Rule for Predicting Uniaxial Magnetic Properties

The analysis of crystal field and spin-orbit coupling effects for high-spin transition metal d^6 ions in the previous section provides a qualitative rule by which to predict what kinds of transition metal ions can exhibit uniaxial magnetic properties. There are three conditions that lead to uniaxial magnetic properties:

a. The coordinate site should have a threefold or higher rotational symmetry so that the d-levels split into the two degen-

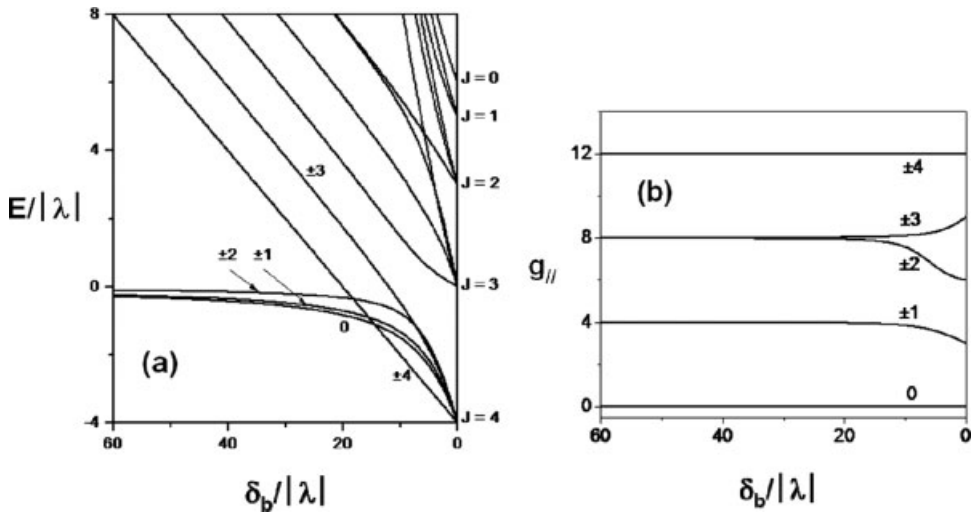

Figure 7. (a) Energies $E_i/|\lambda|$ and (b) g-factors $g_{||}$ calculated for the spin-orbit coupled states of a high-spin d^6 ion at a trigonal prism site ($\delta_a/\delta_b = 0.2$ and $\delta_b > 0$) calculated as a function of $\delta_b/|\lambda|$.

erate sets $\{x^2 - y^2, xy\}$ and $\{xz, yz\}$ plus the nondegenerate set $\{z^2\}$.

b. The d-electron count should be such that one of the two degenerate sets is occupied by three electrons, and hence the ground state is described by two degenerate electronic configurations of nonzero orbital angular momentum.

c. The d-shell should be more than half filled so that the lowest energy of the spin-orbit coupling $\lambda\vec{L}\cdot\vec{S}$ occurs when $\vec{L}$ and $\vec{S}$ are parallel to each other due to the negative spin-orbit coupling constant ($\lambda < 0$).

It is of interest to reconsider the case of a high-spin d^6 ($S = 2$) ion at a linear two-coordinate site from the viewpoint of these conditions. The d-levels of a linear two-coordinate site are split as

$$\{x^2 - y^2, xy\} < \{xz, yz\} < \{z^2\},$$

so that the d-electron configuration is given by

$$(x^2 - y^2, xy)^3 (xz, yz)^2 (z^2)^1.$$

for which $L = 2$. The lowest energy of the spin-orbit coupling $\lambda\vec{L}\cdot\vec{S}$ occurs when $\vec{L}$ and $\vec{S}$ are parallel to each other, so that the ground Kramer's doublet state is given by $M_J = \pm 4$. Since $\Delta M_J = 8$, $g_\perp = 0$ so that the high-spin d^6 ($S = 2$) ion at a linear two-coordinate site leads to uniaxial magnetic properties.

The three conditions (a), (b), and (c) are fulfilled for a high-spin d^6 ($S = 2$) ion at a trigonal bipyramidal site, for which the d-levels are split as

$$\{xz, yz\} < \{x^2 - y^2, xy\} < \{z^2\},$$

which leads to the d-electron configuration

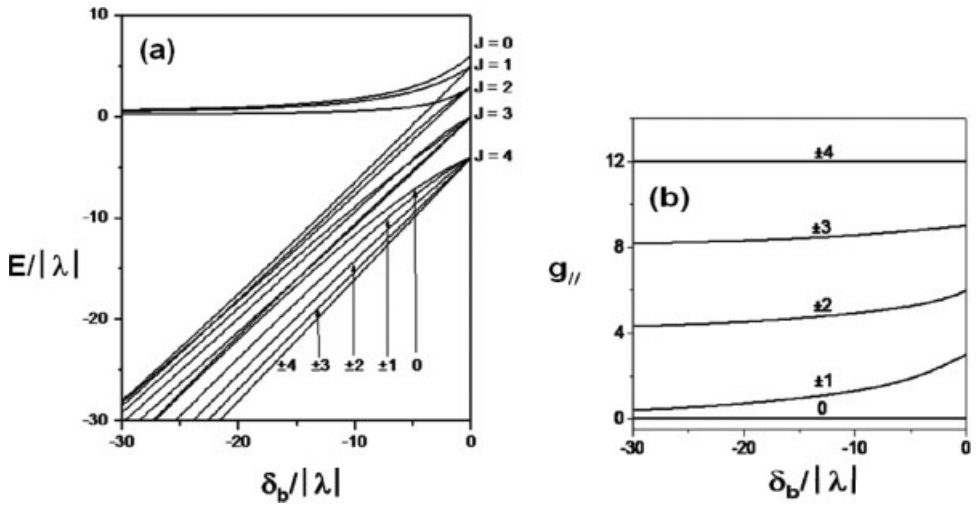

Figure 8. (a) Energies $E_i/|\lambda|$ and (b) g-factors $g_{||}$ calculated for the spin-orbit coupled states of a high-spin d^6 ion at a linear two-coordinate site (i.e., $\delta_a/\delta_b = 1.2$ and $\delta_b < 0$) calculated as a function of $\delta_b/|\lambda|$.

$$(xz, yz)^3(x^2 - y^2, xy)^2(z^2)^1.$$

Then, $L = 1$, and $M_J = \pm 3$ and $\Delta M_J = 6$ for the ground Kramer's doublet state. Consequently, the high-spin d^6 ($S = 2$) ion at a trigonal bipyramidal site should have uniaxial magnetic properties. Such a situation is found for $SrCo_6O_{11}$,[17] which consists of three different cobalt atoms, Co(1), Co(2), and Co(3). The Co(1) and Co(2) atoms are located at octahedral sites, and the Co(3) atoms at trigonal bipyramidal sites. The magnetic properties of $SrCo_6O_{11}$ are uniuaxial, and originate from the high-spin Co^{3+} (d^6) ions at the trigonal bipyramidal sites.[17,18] Another example is found for $LuFe_2O_4$, which consists of hexagonal Fe_2O_4 layers made up of edge-sharing FeO_5 trigonal bipyramids containing $Fe^{2.5+}$ ions. $LuFe_2O_4$ undergoes a charge-order transition below 330 K,[19]

$$2Fe^{2.5+} \rightarrow Fe^{2+} + Fe^{3+},$$

which induces a huge electric polarization along the direction perpendicular to the Fe_2O_4 layers.[19,20] In the charge-ordered state of $LuFe_2O_4$, the high-spin Fe^{2+} ions at the trigonal bipyramidal sites have the electron configuration

$$(xy, yz)^3(x^2 - y^2, xy)^2(z^2)^1$$

with $L = 1$ and $S = 2$, which introduces uniaxial magnetic properties to $LuFe_2O_4$.

The three conditions (a), (b), and (c) are also fulfilled for a high-spin d^6 ($S = 2$) ion at a square pyramidal site.[21] For a high-spin d^6 ion at a square pyramidal site, the d-levels are split as

$$\{xz, yz\} < xy < z^2 < x^2 - y^2,$$

which leads to the d-electron configuration

$$(xz, yz)^3(xy)^1(z^2)^1(x^2 - y^2)^1.$$

Then, $L = 1$, and $M_J = \pm 3$ and $\Delta M_J = 6$ for the ground Kramer's doublet state. Therefore, a high-spin d^6 ($S = 2$) ion at a square pyramidal site is expected to exhibit uniaxial magnetic properties.

Effect of Spin-Orbit Coupling on a Spin Dimer

So far our discussion of spin-orbit coupling has been limited to the Hamiltonian of a single spin site. We now consider a spin dimer consisting of two separate spin sites under the assumption that the spin-orbit coupling constant at each spin site is λ. In general, the spin-orbit coupling between the sites (i.e., $\lambda\hat{S}_1 \cdot \hat{L}_2 + \lambda\hat{S}_2 \cdot \hat{L}_1$) is negligible. The effect of spin-orbit coupling on a spin dimer can be described by the Dzyaloshinsky-Moriya approach[22] when the orbital ground state is nondegenerate, and by the Lines' approach[7] when the ground state is degenerate.

Cases of Nondegenerate Ground States

The effective spin Hamiltonian for a spin dimer can be written as[23]

$$\hat{H} = -J\hat{S}_1 \cdot \hat{S}_2 + \hat{D} \cdot (\hat{S}_1 \times \hat{S}_2) + \hat{S}_1 \cdot \Gamma \cdot \hat{S}_2, \tag{77}$$

where the first term describes the isotropic interaction, the second term the antisymmetric interaction, and the third term the anisotropic interaction. In the following we examine each term separately.

Isotropic Interaction

For simplicity, let us consider a dimer with a single electron (i.e., spin-1/2) at each site. In the absence of the spin-orbit coupling and the interaction between the sites, the total Hamiltonian can be written as the sum of two one-electron Hamiltonians, namely,

$$\hat{H}_0 = \hat{h}_1 + \hat{h}_2, \tag{78}$$

where

$$\hat{h}_1 = \frac{\hat{p}_1^2}{2} + V(|\vec{r}_1 - \vec{R}_1|),$$

$$\hat{h}_2 = \frac{\hat{p}_2^2}{2} + V(|\vec{r}_2 - \vec{R}_2|).$$

$\vec{R}_1$ and $\vec{R}_2$ are the position vectors of the nuclei 1 and 2, respectively, and $V(|\vec{r}_1 - \vec{R}_1|)$ and $V(|\vec{r}_2 - \vec{R}_2|)$ are the local central fields at the spin sites 1 and 2, respectively. The eigenvalue equations of $\hat{h}_1$ and $\hat{h}_2$ are written as

$$\begin{aligned} \hat{h}_1|n_1\rangle &= E_{n_1}|n_1\rangle, \\ \hat{h}_2|n_2\rangle &= E_{n_2}|n_2\rangle. \end{aligned} \tag{79}$$

Then, the eigenfunction of the $\hat{H}_0$ can be written as

$$|\Psi_0\rangle = |n_1\rangle|n_2\rangle, \tag{80}$$

and

$$\hat{H}_0|\Psi_0\rangle = (\hat{h}_1 + \hat{h}_2)|n_1\rangle|n_2\rangle = (E_{n1} + E_{n2})|n_1\rangle|n_2\rangle = E_0|\Psi_0\rangle. \tag{81}$$

The fact that the total wave function is the product of the two wavefunctions, eq. (80), is the consequence of the independence of each site, i.e., no interaction between the sites. To introduce the interaction between the sites, we add the electron-electron repulsion term

$$\hat{h}_{12} = \frac{1}{|\vec{r}_1 - \vec{r}_2|} = \frac{1}{r_{12}} \tag{82}$$

into the total Hamiltonian. Then the total energy of the system becomes

$$\begin{aligned}\langle n_1|\langle n_2|\hat{H}|n_1\rangle|n_2\rangle &= \langle n_1|\langle n_2|\hat{H}_0+\hat{h}_{12}|n_1\rangle|n_2\rangle \\ &= \langle n_1|\langle n_2|\hat{H}_0|n_1\rangle|n_2\rangle + \langle n_1|\langle n_2|\hat{h}_{12}|n_1\rangle|n_2\rangle \\ &= E_0 + \langle n_1|\langle n_2|\hat{h}_{12}|n_1\rangle|n_2\rangle\end{aligned} \tag{83}$$

Namely, the change of the ground state energy due to the interaction between the sites is given by

$$\langle n_1|\langle n_2|\hat{h}_{12}|n_1\rangle|n_2\rangle. \tag{84}$$

This energy term can be replaced with $-J\,\hat{S}_1\cdot\hat{S}_2$, i.e.,

$$\langle n_1|\langle n_2|\hat{h}_{12}|n_1\rangle|n_2\rangle \approx -J\hat{S}_1\cdot\hat{S}_2\,, \tag{85}$$

where J is a function of the orbitals n_1 and n_2.[23] Namely, the term $-J\,\hat{S}_1\cdot\hat{S}_2$ is a consequence of $\hat{h}_{12}$, i.e., the interaction between the electrons of the two sites. The interaction energy $-J\,\hat{S}_1\cdot\hat{S}_2$ is determined by two factors, the spin exchange parameter J as well as the spins at both sites S_1 and S_2. In other words, J has absorbed all the information about the electronic structure of the dimer. The spins S_1 and S_2 determine the structure of the energy spectrum, while J determines the energy gaps between the states.

Antisymmetric Interaction

The Hamiltonian $\hat{H}_0+\hat{h}_{12}$ has not included the spin-orbit coupling. Recalling the assumption that the spin-orbit coupling between the sites (i.e., $\lambda\hat{S}_1\cdot\hat{L}_2+\lambda\hat{S}_2\cdot\hat{L}_1$) is negligible, we may write

$$\hat{H}_{\mathrm{SO}} = \lambda\hat{S}\cdot\hat{L} = \lambda(\hat{S}_1+\hat{S}_2).(\hat{L}_1+\hat{L}_2) \approx \lambda\hat{S}_1\cdot\hat{L}_1+\lambda\hat{S}_2\cdot\hat{L}_2\,, \tag{86}$$

Then the total Hamiltonian becomes

$$\hat{H} = \hat{H}_0+\hat{h}_{12}+\lambda\hat{S}_1\cdot\hat{L}_1+\lambda\hat{S}_2\cdot\hat{L}_2\,. \tag{87}$$

Using the eigenfunctions of $\hat{H}_0$ as the zero-order wavefunction and $\hat{h}_{12}+\lambda\hat{S}_1\cdot\hat{L}_1+\lambda\hat{S}_2\cdot\hat{L}_2$ as the perturbation, one can derive the second order perturbation energy as (The first-order perturbation energy vanishes because the assumption of the nondegenerate orbital ground state implies $\langle L\rangle = 0$)[22b,c]

$$\Delta E^{(2)} = \left[\lambda J(\vec{l}_1-\vec{l}_2)\right](\hat{S}_1\times\hat{S}_2) = \vec{D}\cdot(\hat{S}_1\times\hat{S}_2)\,, \tag{88}$$

where

$$\begin{aligned}\vec{l}_1 &= i\sum_{n_1'}^{\text{excited orbitals}}\frac{<n_1|\hat{L}_1|n_1'>}{E_{n_1}-E_{n_1'}}, \\ \vec{l}_2 &= i\sum_{n_2'}^{\text{excited orbitals}}\frac{<n_2|\hat{L}_2|n_2'>}{E_{n_2}-E_{n_2'}}.\end{aligned} \tag{89}$$

As discussed in "Electronic structure and orbital angular momentum" section, the terms $\vec{l}_1$ and $\vec{l}_2$ can be interpreted as the unquenched orbital angular momentum at the sites 1 and 2, respectively. Then the Dzyaloshinsky-Moriya vector $\vec{D}$ is the consequence of the difference in the unquenched orbital angular momenta on the two magnetic sites. $\vec{D}\cdot(\hat{S}_1\times\hat{S}_2)$ is usually called the antisymmetric interaction. When $\hat{S}_1$ and $\hat{S}_2$ are switched, the sign of $\hat{S}_1\times\hat{S}_2$ changes, i.e., $\hat{S}_2\times\hat{S}_1 = -\hat{S}_1\times\hat{S}_2$. Note that the sign of $\vec{D}=[\lambda J(\vec{l}_1-\vec{l}_2)]$ also changes when the sites 1 and 2 are switched. Therefore, the sign of the overall $\vec{D}\cdot(\hat{S}_1\times\hat{S}_2)$ is independent of the site index.

The vector $\vec{D}$ has the same direction as does the difference vector $((\vec{l}_1-\vec{l}_2))$, and has the following properties[22c]:

a. When a center of inversion is at the midpoint between the sites 1 and 2, $\vec{D}=0$.
b. When a mirror plane perpendicular to the line segment 1–2 between the sites 1 and 2 bisects the segment, $\vec{D}$ is parallel to the mirror plane.
c. When there is a mirror plane containing the sites 1 and 2, $\vec{D}$ is perpendicular to the mirror plane.
d. When a two-fold rotation axis perpendicular to the line segment 1–2 passes through its midpoint, $\vec{D}$ is perpendicular to the twofold axis.
e. When there is an n-fold axis ($n\geq 2$) along the line segment 1–2, $\vec{D}$ is parallel to the line segment.

While the direction of the vector $\vec{D}$ is determined by $(\vec{l}_1-\vec{l}_2)$, the magnitude of $\vec{D}$ is proportional to $\lambda/\Delta E$, where ΔE accounts for the crystal field splitting. The value of $\vec{D}\cdot(\hat{S}_1\times\hat{S}_2)$ is equal to the volume of the parallelepiped made up of the three vectors $\vec{D}$, $\hat{S}_1$, and $\hat{S}_2$. When the lengths of these vectors are fixed, the absolute volume reaches its maximum when the three vectors are perpendicular to each other. Therefore, given a certain direction of $\vec{D}$, the term $\vec{D}\cdot(\hat{S}_1\times\hat{S}_2)$ tends to align the two spin vectors $\hat{S}_1$ and $\hat{S}_2$ perpendicular to each other and to the vector $\vec{D}$ (under the assumption that $\vec{D}<0$).

To calculate the matrix elements of the antisymmetric term, it is convenient to choose the coordinate system with the z-axis parallel to the vector $\vec{D}$. Then $D_x=D_y=0$, $D_z=|\vec{D}|$, and

$$\vec{D}\cdot(\hat{S}_1\times\hat{S}_2) = D_z(\hat{S}_{1x}\hat{S}_{2y}-\hat{S}_{1y}\hat{S}_{2x}) = (\mathrm{i}/2)D_z(\hat{S}_{1+}\hat{S}_{2-}-\hat{S}_{1-}\hat{S}_{2+}). \tag{90}$$

A dimer with $S_1=S_2=1/2$ described by the Hamiltonian $-J\,\hat{S}_1\cdot\hat{S}_2$ has the singlet and triplet states given below

$$\begin{aligned}|S\rangle = |S\,M_S\rangle = |0\,0\rangle &= \sqrt{1/2}(|\uparrow\rangle_1|\downarrow\rangle_2-|\downarrow\rangle_1|\uparrow\rangle_2), \\ |T\rangle = |S\,M_S\rangle = |1\,0\rangle &= \sqrt{1/2}(|\uparrow\rangle_1|\downarrow\rangle_2+|\downarrow\rangle_1|\uparrow\rangle_2).\end{aligned} \tag{91}$$

These states interact under the term the term $\vec{D}\cdot(\hat{S}_1\times\hat{S}_2)$ because the matrix elements

$$\langle S|\vec{D}\cdot(\hat{S}_1\times\hat{S}_2)|T\rangle = -\langle T|\vec{D}\cdot(\hat{S}_1\times\hat{S}_2)|S\rangle = (\mathrm{i}/2)D_z \tag{92}$$

are nonzero. Suppose now that a spin dimer with $S_1=S_2=1/2$ are described by the Hamiltonian $\hat{H}=-J\,\hat{S}_1\cdot\hat{S}_2+\vec{D}\cdot(\hat{S}_1\times\hat{S}_2)$. Then, for the states $|S\rangle$ and $|T\rangle$, we obtain the following matrix elements,

$$\begin{aligned}\langle S|\hat{H}|S\rangle &= 3J/4, \quad \langle T|\hat{H}|T\rangle = -J/4, \\ \langle S|\hat{H}|T\rangle &= (\mathrm{i}/2)D_z, \quad \langle T|\hat{H}|S\rangle = -(\mathrm{i}/2)D_z.\end{aligned} \tag{93}$$

Since $\langle S|\hat{H}|T\rangle$ does not vanish, the states $|S\rangle$ and $|T\rangle$ will interact to generate new states $|S'\rangle$ and $|T'\rangle$, respectively. The energy difference between the states $|S\rangle$ and $|T\rangle$ is J, while $|D_z| \ll |J|$ in general. Therefore, given the quantity τ defined as

$$\tau = \frac{D_z}{2J}, \tag{94}$$

the state $|S'\rangle$ and its energy $E(S')$ can be expressed as

$$\begin{aligned} |S'\rangle &\approx (1 - \tau^2/2|S\rangle - i\tau|T\rangle, \\ E(S') &\approx 3J/4 + (D_z)^2/4J\,, \end{aligned} \tag{95}$$

Likewise, the state $|T'\rangle$ and its energy $E(T')$ are written as

$$\begin{aligned} |T'\rangle &\approx (1 - \tau^2/2)|T\rangle + i\tau|S\rangle, \\ E(T') &\approx -J/4 - (D_z)^2/4J. \end{aligned} \tag{96}$$

The state $|S'\rangle$ has $|S\rangle$ as the major component with a small contribution of $|T\rangle$, while the state $|T'\rangle$ has $|T\rangle$ as the major component with a small contribution of $|S\rangle$. Thus, the antisymmetric term $\vec{D}\cdot(\hat{S}_1\times\hat{S}_2)$ leads to a weak mixing between the singlet and triplet states, $|S\rangle$ and $|T\rangle$. In essence, such a mixing of nonzero-moment states into the zero-moment state is responsible for the occurrence of spin canting and hence weak ferromagnetism in an antiferromagnetic system.

Following the same procedure one may readily obtain all the matrix elements and consequently the energies of the eigenstates of the isotropic and antisymmetric Hamiltonian for various spin dimers. All the nonzero matrix elements for spin dimers with $S_1 = S_2 =$ 1/2, 1, 3/2, 2, and 5/2 are listed in the ref. 24. Using these matrix elements, the energies in units of J can be determined in terms of the ratio $|D_z/J|$. The analytical and pseudo-analytical expressions of the eigenvalues are also given in the ref. 24. In general, under the antisymmetry Hamiltonian, all the states with same M_S can interact with each other although their total spin S may differ.

Anisotropic Interaction

As discussed above, the isotropic term $-J\,\hat{S}_1\cdot\hat{S}_2$ is induced by the Coulomb interaction between the electrons at the two sites 1 and 2, and the antisymmetric term $\vec{D}\cdot(\hat{S}_1\times\hat{S}_2)$ is a consequence of the second order perturbation of the Coulomb and spin-orbit interaction (i.e., $\hat{h}_{12} + \lambda\hat{S}_1\cdot\hat{L}_1 + \lambda\hat{S}_2\cdot\hat{L}_2$). If we employ the same Hamiltonian, then the third order perturbation energy is given by

$$\begin{aligned} \Delta E^{(3)} = &\sum_{n_1'}^{\substack{\text{excited orbitals}\\ \text{on site 1}}} \frac{\langle \mathrm{n}_1|\lambda\hat{S}_1\cdot\hat{L}_1|n_1'\rangle(-J\hat{S}_1\cdot\hat{S}_2)\langle n_1'|\lambda\hat{S}_1\cdot\hat{L}_1|n_1\rangle}{(E_{n_1'} - E_{n_1})^2} \\ &+ \sum_{n_2'}^{\substack{\text{excited orbitals}\\ \text{on site 2}}} \frac{\langle \mathrm{n}_2|\lambda\hat{S}_2\cdot\hat{L}_2|n_2'\rangle(-J\hat{S}_1\cdot\hat{S}_2)\langle n_2'|\lambda\hat{S}_2\cdot\hat{L}_2|n_2\rangle}{(E_{n_2'} - E_{n_2})^2}\,. \end{aligned} \tag{97}$$

After some algebra, this can be simplified as[25]

$$\Delta E^{(3)} = \sum_{\mu,\nu}^{x,y,z} \hat{S}_{1\mu}\Gamma_{\mu\nu}\hat{S}_{2\nu} = \hat{S}_1\cdot\Gamma\cdot\hat{S}_2, \tag{98}$$

where

$$\begin{aligned} \Gamma_{\mu\nu} &= \lambda^2\left[\gamma^{(1)} - \gamma_{\mu\nu}^{(1)}\right] + \lambda^2\left[\gamma^{(2)} - \gamma_{\mu\nu}^{(2)}\right], \\ \gamma_{\mu\nu}^{(1)} &= \sum_{n_1'}^{\substack{\text{excited orbitals}\\ \text{on site 1}}} K_{n_1'n_2}\frac{< n_1|\hat{L}_{1\mu}|n_1' >< n_1'|\hat{L}_{1\nu}|n_1 >}{(E_{n_1'} - E_{n_1})^2}, \\ \gamma_{\mu\nu}^{(2)} &= \sum_{n_2'}^{\substack{\text{excited orbitals}\\ \text{on site 2}}} K_{n_2'n_1}\frac{< n_2|\hat{L}_{2\mu}|n_2' >< n_2'|\hat{L}_{2\nu}|n_2 >}{(E_{n_2'} - E_{n_2})^2}, \\ \gamma^{(1)} &= \left[\gamma_{xx}^{(1)} + \gamma_{yy}^{(1)} + \gamma_{zz}^{(1)}\right]/3, \\ \gamma^{(2)} &= \left[\gamma_{xx}^{(2)} + \gamma_{yy}^{(2)} + \gamma_{zz}^{(2)}\right]/3. \end{aligned} \tag{99}$$

Here $K_{n_1'n_2}$ is the exchange integral between the states n'_1 (the excited state orbital of the site 1) and n_2 (the ground state orbital of the site 2), while $K_{n_2'n_1}$ is the exchange integral between the states n'_2 (the excited state orbital of the site 2) and n_1 (the ground state orbital of the site 1).

The Γ matrix has a form similar to the Λ matrix discussed in "Effective spin approach and g-factor" section. The diagonal elements $\Gamma_{\mu\mu}$ are related to the unquenched orbital angular momentum along the μ direction. Obviously, when the unquenched orbital angular momentum along each direction is same, $\Gamma_{\mu\mu} = 0$ Therefore, the Γ matrix describes the difference in the unquenched angular momenta along the three directions. As a consequence, $\hat{S}_1\cdot\Gamma\cdot\hat{S}_2$ is termed the anisotropic term.

Cases of Degenerate Ground States

In deriving the effective Hamiltonian terms $\vec{D}\cdot(\hat{S}_1\times\hat{S}_2)$ and $\hat{S}_1\cdot\Gamma\cdot\hat{S}_2$ in eq. (77), it was assumed that the ground state orbital is a nondegenerate singlet. Thus, the orbital angular momentum of the ground state vanishes, and only the excited states introduced into the ground state by the second-order and third-order perturbations give rise to a nonzero angular momentum. In case when the ground state orbitals are degenerate as in $CoCl_2$, which contains high-spin Co^{2+} (d^7) ions in slightly distorted octahedral environments, one may follow the pseudo-spin approach of Lines[7] to study the magnetic anisotropy.

In "High-spin d^7 ions at octahedral sites" section, we showed that the ground state of $CoCl_2$ is Kramer's doublet state, the wavefunctions, ψ_+ and ψ_-, of which are written as in eq. (63). Now we are in a position to describe the magnetic anisotropy of $CoCl_2$. First, it is necessary to examine how adjacent Co^{2+} ions interact in terms of their ground Kramers' doublet states. For this purpose, Lines employed the functions ψ_+ and ψ_-,

$$\begin{aligned} \psi_+ &= c_1\left|-1\,\tfrac{3}{2}\right\rangle + c_2\left|0\,\tfrac{1}{2}\right\rangle + c_3\left|1\,-\tfrac{1}{2}\right\rangle, \\ \psi_- &= c_1\left|1\,-\tfrac{3}{2}\right\rangle + c_2\left|0\,-\tfrac{1}{2}\right\rangle + c_3\left|-1\tfrac{1}{2}\right\rangle, \end{aligned}$$

as basis functions to determined the matrix elements

$$\left\langle \psi_i | \hat{S}_\mu | \psi_j \right\rangle \quad (i,j = +,-; \mu = x,y,z).$$

By using the relationships $\hat{S}_x = (\hat{S}_+ + \hat{S}_-)/2$ and $\hat{S}_y = (\hat{S}_+ - \hat{S}_-)/2\mathrm{i}$, it is straightforward to find the following matrix representations of $\hat{S}_x$, $\hat{S}_y$, and $\hat{S}_z$.

$$\begin{aligned} \mathbf{S}_x &= \begin{pmatrix} 0 & q \\ q & 0 \end{pmatrix}, \\ \mathbf{S}_y &= \begin{pmatrix} 0 & -iq \\ iq & 0 \end{pmatrix}, \\ \mathbf{S}_z &= \begin{pmatrix} p & 0 \\ 0 & p \end{pmatrix}, \end{aligned} \tag{100}$$

where the constants p and q are given by[7]

$$\begin{aligned} p &= \tfrac{3}{2}c_1^2 + \tfrac{1}{2}c_2^2 - \tfrac{1}{2}c_3^2, \\ q &= c_2^2 + \sqrt{3}c_1c_3 \end{aligned} \tag{101}$$

It is recalled that in terms of the spin states $|+1/2 + 1/2\rangle$ and $|+1/2 - 1/2\rangle$ of a single electron as basis functions, the spin-half operators $\hat{S}_x$, $\hat{S}_y$, and $\hat{S}_z$ have the matrix representations given below.

$$\begin{aligned} \mathbf{S}_x &= \frac{1}{2}\begin{pmatrix} 0 & 1 \\ 1 & 0 \end{pmatrix}, \\ \mathbf{S}_y &= \frac{1}{2}\begin{pmatrix} 0 & -i \\ i & 0 \end{pmatrix}, \\ \mathbf{S}_z &= \frac{1}{2}\begin{pmatrix} 1 & 0 \\ 0 & 1 \end{pmatrix}. \end{aligned} \tag{102}$$

Therefore, the spin operators $\hat{S}_x$, $\hat{S}_y$, and $\hat{S}_z$ for the ground Kramers' doublet state can be rewritten as,

$$\begin{aligned} \hat{S}_x &= 2q\hat{s}_x, \\ \hat{S}_y &= 2q\hat{s}_y, \\ \hat{S}_z &= 2p\hat{s}_z \end{aligned} \tag{103}$$

The above relationship enables one to describe the anisotropic spin exchange interaction between nearest neighbor Co^{2+} ions of $CoCl_2$ formally by using the Heisenberg Hamiltonian $\hat{H} = -J\,\hat{S}_1 \cdot \hat{S}_2$. If the operators $\hat{S}_1$ and $\hat{S}_2$ are replaced with the pseudo-spin operators, one obtains the effective spin Hamiltonian

$$\hat{H} = -J\left[(2p)^2\hat{s}_{1z}\hat{s}_{2z} + (2q)^2\left(\hat{s}_{1x}\hat{s}_{2x} + \hat{s}_{1y}\hat{s}_{2y}\right)\right], \tag{104}$$

which is rewritten as

$$\hat{H} = -J'(\hat{s}_1 \cdot \hat{s}_2) + D'(\hat{s}_{1x}\hat{s}_{2x} + \hat{s}_{1y}\hat{s}_{2y}) \tag{105}$$

where

$$\begin{aligned} J' &= (2q)^2 J, \\ D' &= [(2q)^2 - (2p)^2]J. \end{aligned} \tag{106}$$

The *D*'/*J*' ratio can be deduced experimentally using magnetic susceptibility data, and provides a measure of the extent of the anisotropy in the spin exchange interaction.

It is important to notice that the Heisenberg Hamiltonian $\hat{H} = -J\,\hat{S}_1 \cdot \hat{S}_2$ describes isotropic spin exchange interactions when the spin operators $\hat{S}_1$ and $\hat{S}_2$ refer to pure spin operators. However, this Hamiltonian can be employed to describe anisotropic interactions if $\hat{S}_1$ and $\hat{S}_2$ are replaced with the pseudo-spin operators, because the effect of spin-orbit coupling and crystal field has already been included in the pseudo-spin operators at each spin site. The pseudo-spin approach is convenient because the anisotropy of a magnetic system at low temperatures depends primarily on the ground orbital state of each magnetic ion, and because the ground orbital state can be easily identified by analyzing how the crystal field and spin-orbit coupling split the ground orbital state of a free magnetic ion.

Properties of Magnetic Solids Induced by Spin Orbit Coupling

Direction of Magnetization

In a magnetic solid the magnetic moment of each spin site results from the spin moment interacting with the unquenched orbital moment under the spin-orbit coupling $\hat{H}_{SO} = \lambda\hat{L} \cdot \hat{S}$. An important consequence of this interaction is that the magnetic moment of each spin site gets a preferred orientation in space with respect to the crystal lattice. It is important to understand this aspect of spin-orbit coupling in magnetic solids. Note that the term $\hat{L} \cdot \hat{S}$ is typically written as

$$\hat{L} \cdot \hat{S} = \hat{L}_z\hat{S}_z + \hat{L}_x\hat{S}_x + \hat{L}_y\hat{S}_y = \hat{L}_z\hat{S}_z + \frac{1}{2}\hat{L}_+\hat{S}_- + \frac{1}{2}\hat{L}_-\hat{S}_+, \tag{107}$$

but this expression does not provide explicit information concerning how to think about the orientation of the magnetization direction in space. A more informative expression of $\hat{L} \cdot \hat{S}$ is obtained by explicitly considering the magnetization direction of the spin moment, $\hat{n}(\theta, \phi)$, where θ and ϕ as the azimuthal and polar angles of the magnetization direction with respect to the coordinate system of the magnetic solid. Then, the $\hat{L} \cdot \hat{S}$ term is written as[26]

$$\begin{aligned} \hat{L} \cdot \hat{S} = \hat{S}_n\Big(\hat{L}_z \cos\theta + \frac{1}{2}\hat{L}_+e^{-i\phi}\sin\theta + \frac{1}{2}\hat{L}_-e^{i\phi}\sin\theta\Big) \\ + \frac{1}{2}\hat{S}_+\Big(-\hat{L}_z\sin\theta - \hat{L}_+e^{-i\phi}\sin^2\frac{\theta}{2} + \hat{L}_-e^{i\phi}\cos^2\frac{\theta}{2}\Big). \\ + \frac{1}{2}\hat{S}_-\Big(-\hat{L}_z\sin\theta + \hat{L}_+e^{-i\phi}\cos^2\frac{\theta}{2} - \hat{L}_-e^{i\phi}\sin^2\frac{\theta}{2}\Big) \end{aligned} \tag{108}$$

Note that this expression makes use of two different coordinate systems, i.e., one coordinate system (x, y, and z) for the orbital angular momentum operators, and another coordinate system (x', y', and z') for the spin angular momentum operators such that the z'-axis is aligned along the $\hat{n}(\theta, \phi)$ direction, i.e.,

$\hat{S}_n = \hat{S}_{z'}$, $\hat{S}_+ = \hat{S}_{x'} + i\hat{S}_{y'}$ and $\hat{S}_- = \hat{S}_{x'} - i\hat{S}_{y'}$. For the derivation of eq. (108), see Appendix. This expression shows how spin-orbit coupling depends on the magnetization direction, and hence provides information about what magnetization direction is energetically favored by spin-orbit coupling for a given magnetic solid. To determine theoretically the easy-axis direction of a magnetic solid, its total energy including spin-orbit coupling interactions should be calculated as a function of the magnetization direction.[27] Then, the easy-axis direction is the magnetization direction with the lowest total energy. Experimentally, neutron diffraction refinements at a very low temperature provide information about the magnitudes and orientations of the moments at the spin sites of a magnetic solid.

For a qualitative discussion of spin-orbit coupling and magnetization direction, the "spin-conserving" term of $\hat{L} \cdot \hat{S}$, i.e., the first line of eq. (108), is important. Let us define the spin-conserving part of the spin-orbit coupling Hamiltonian, $\hat{H}_{SO}^{sc}$, as

$$\hat{H}_{SO}^{sc} \equiv \lambda \hat{S}_n \left(\hat{L}_z \cos\theta + \frac{1}{2}\hat{L}_+ e^{-i\phi} \sin\theta + \frac{1}{2}\hat{L}_- e^{i\phi} \sin\theta \right). \quad (109)$$

In general, the spin-orbit coupling operator $\hat{H}_{SO}$ leads to nonzero interactions between states with different spin and orbital momenta. The $\hat{H}_{SO}^{sc}$ term leads to nonzero interactions only between states with a same spin moment S but with different orbital moments L. The second and third lines of eq. (108) lead to nonzero interactions only between states with different spin moments S. From the viewpoint of first principles electronic structure calculations, states with a given spin moment are generally well separated in energy from those with a different spin moment. In general, therefore, the spin-orbit coupling from the spin-conserving term will be more important than that from the nonspin-conserving terms of $\hat{H}_{SO}$.

Some Important Consequences of Spin Orbit Coupling

Occurrence of an Insulating Gap

Let us examine how spin-orbit coupling, $\hat{H}_{SO} = \lambda \hat{L} \cdot \hat{S}$, affects the t_{2g} level of an Os^{7+} (d^1) ion in each OsO_6 octahedron found in the double perovskite Ba_2NaOsO_6,[28–30] which consists of isolated OsO_6 octahedra. For this case, $\lambda > 0$, because the t_{2g} level of an Os^{7+} (d^1) ion is less than half-filled. Due to electron correlation the up-spin t_{2g} level is well separated in energy from the down-spin t_{2g} level, so that we consider only how the partially occupied up-spin t_{2g} level will be split by spin-orbit coupling on the basis of degenerate perturbation theory.[3,29] The latter requires the construction of the matrix elements $\langle i|\hat{H}_{SO}|j\rangle$ (i, j = xy, xz, yz).

The angular parts of the d orbitals are described by the spherical harmonics as shown below

$$\begin{aligned} z^2 &\propto Y_2^0, \\ x^2 - y^2 &\propto (1/\sqrt{2})(Y_2^2 + Y_2^{-2}), \\ xy &\propto (-i/\sqrt{2})(Y_2^2 - Y_2^{-2}), \\ yz &\propto (i/\sqrt{2})(Y_2^1 + Y_2^{-1}), \\ xz &\propto (-1/\sqrt{2})(Y_2^1 - Y_2^{-1}). \end{aligned} \quad (110)$$

Thus, it is readily seen that the nonzero matrix elements of $\langle i|\hat{H}_{SO}|j\rangle$ result only from the spin-conserving part $\langle i|\hat{H}_{SO}^{sc}|j\rangle$, which is found to be

$$(\lambda/2)\begin{pmatrix} 0 & \sin\theta\sin\phi & -\sin\theta\cos\phi \\ -\sin\theta\sin\phi & 0 & \cos\theta \\ \sin\theta\cos\phi & -\cos\theta & 0 \end{pmatrix}. \quad (111)$$

Diagonalization of this matrix leads to the three spin-orbit coupled states with the eigenvalues E_i (i = 1, 2, 3),

$$E_1 = -\lambda/2, \quad E_2 = 0, \quad \text{and} \quad E_3 = \lambda/2, \quad (112)$$

in units of $\hbar$. The eigenfunctions ψ_i associated with these eigenvalues are given by

$$\begin{aligned} \psi_1 &= \frac{\sqrt{2}}{2}[(\sin\theta)xy + (i\sin\theta - \cos\theta\cos\phi)yz \\ &\quad - (i\cos\phi + \cos\theta\sin\phi)xz] \\ \psi_2 &= (\cos\theta)xy + (\sin\theta\cos\phi)yz + (\sin\theta\sin\phi)xz \\ \psi_3 &= \frac{\sqrt{2}}{2}[(\sin\theta)xy - (i\sin\theta + \cos\theta\cos\phi)yz \\ &\quad + (i\cos\phi - \cos\theta\sin\phi)xz] \end{aligned} \quad (113)$$

Since the eigenvalues E_1, E_2, and E_3 are independent of the magnetization direction, the Os^{7+} (d^1) ions of the OsO_6 octahedra are expected to have no magnetic anisotropy to a first approximation. Given the Hamiltonoian $\hat{H}_{SO} = \lambda \hat{L} \cdot \hat{S}$ with S = 1/2, the states ψ_1, ψ_2, and ψ_3 have the orbital moments $L = -1$ μ_B, 0 and 1 μ_B, respectively, along the magnetization direction, according to their eigenvalues.

An Os^{7+} (d^1) ion occupies only ψ_1, which is separated from the unoccupied levels ψ_2 and ψ_3 with an energy gap. This split of the t_{2g} level induced spin-orbit coupling, together with the effect of electron correlation that increases the energy separation between the occupied and unoccupied levels, is found crucial for the occurrence of an insulating band gap in Ba_2NaOsO_6.[29] The occupation of ψ_1 leads to the orbital moment of -1 μ_B for the spin-orbit coupled state. First principles density functional theory (DFT) calculations for Ba_2NaOsO_6 including spin-orbit coupling and electron correlation show[29] the orbital moment of -0.35 μ_B, considerably smaller in magnitude than -1 μ_B. This reflects the fact that the t_{2g} orbitals of an OsO_6 octahedron in Ba_2NaOsO_6 are not pure 5d orbitals of Os, xz, yz, and xy, but have almost equal contributions from the Os 5d and the O 2p states. Thus, an orbital moment of approximately -0.5 μ_B should be expected from the occupation of the up-spin t_{2g} band associated related to ψ_1. Consequently, the total moment of Ba_2NaOsO_6 per formula should be smaller than the spin-only value of 1 μ_B because the orbital and spin moments should be antiparallel to each other for any $\lambda > 0$ case. Indeed, the zero-field moments determined from the magnetization study of Ba_2NaOsO_6 is considerably smaller than 1 μ_B (i.e., $\sim$0.2 μ_B).[28]

The above discussion implicitly assumed that orbital ordering or Jahn-Teller distortion is absent in the OsO_6 octahedra of Ba_2NaOsO_6. The presence of weak orbital ordering in the OsO_6

octahedra, suggested by experiment,[28] does not change the above discussion.

In-Plane Anisotropy of a High-Spin Fe^{2+} (d^6) Ion at a Square Planar Site

As another example for the use of eq. (109), we examine the magnetic structure of the layered compound $SrFeO_2$.[31] In this compound the planar FeO_2 layers made up of corner-sharing FeO_4 square planes stack along the *c*-direction and are separated by Sr^{2+} ions. Powder neutron diffraction experiments[31] showed that the spin moments of the high-spin Fe^{2+} (d^6) ions present in this compound are parallel to the FeO_2 layer, i.e., parallel to the ab-plane. First principles DFT calculations for $SrFeO_2$ including spin-orbit coupling and electron correlation found[32] that the state with the spin moments parallel to the ab-plane is indeed more stable than that with spin moment perpendicular to the ab-plane. To account for this ab-plane magnetic anisotropy, we first note that, according to first principles DFT calculations for $SrFeO_2$,[32] the electron configuration of a Fe^{2+} (d^6) ion in each FeO_4 square plane is given by

$$(z^2)^2(xz, yz)^1(xy)^1(x^2 - y^2)^1. \tag{114}$$

Thus, in the down-spin energy levels, the HOMO is the z^2 level while the LUMO is the (xz, yz) levels.[32] For square planar coordination environment, the HOMO-LUMO energy difference is small. The energy lowering associated with the HOMO-LUMO interaction induced by spin-orbit coupling depends on the matrix elements,

$$\langle z^2|\hat{H}^{sc}_{SO}|xz\rangle \quad \text{and} \quad \langle z^2|\hat{H}^{sc}_{SO}|yz\rangle. \tag{115}$$

Using eq. (110) it can be readily seen that the nonzero parts of these matrix elements depend on the magnetization direction as

$$\langle z^2|\hat{H}^{sc}_{SO}|xz\rangle \propto \langle z^2|\hat{H}^{sc}_{SO}|yz\rangle \propto \langle Y^0_2|\hat{L}_-|Y^1_2\rangle \sin\theta. \tag{116}$$

Therefore, the energy lowering induced by spin-orbit coupling is maximum, when $\theta = 90^\circ$, i.e., when the magnetization direction is parallel to the ab-plane. This is in agreement with the experimental finding.[31]

Ferroelectricity Arising from Spiral Spin Order

The cuprates $LiCu_2O_2$ and $LiCuVO_4$ consist of CuO_2 ribbon chains that are made up of edge-sharing CuO_4 square planes with spin-1/2 ions Cu^{2+}. In these CuO_2 ribbon chains (Fig. 9a), the nearest-neighbor spin exchange J_{nn} is ferromagnetic while the next-nearest-neighbor spin exchange J_{nnn} is antiferromagnetic,[33] so that the intra-chain spin exchange interactions are frustrated. Furthermore, the $|J_{nnn}/J_{nn}|$ ratio is greater than 0.25,[33] which makes the spins adopt a spiral spin arrangement[34] in each CuO_2 ribbon chain below a certain temperature. The spiral spin arrangement in the CuO_2 chains removes the inversion symmetry of the crystal lattice and hence introduces nonzero electric polarization (i.e., ferroelectricity) into the crystal lattice of $LiCu_2O_2$ and $LiCuVO_4$. This example of multiferroicity,[35] i.e., emergence of ferroelectricity induced by magnetic ordering, is caused by spin-orbit coupling.[33,36]

To probe how spin-orbit coupling induces asymmetric charge distribution in a CuO_2 ribbon chain, it is convenient to employ the coordinate system shown in Figure 9a, where the *x*-axis runs along the chain direction while the CuO_4 square planes lie in the xy-plane. Then, the magnetic orbital of a CuO_4 square plane is given by the xy orbital (Note that in the Cartesian coordinate system of Figure 1a, this orbital is $x^2 - y^2$.). From the viewpoint of local bonding around each Cu^{2+} site, the spin-orbit coupling at each Cu site mixes into the xy hole-state other d hole-states (i.e., the $x^2 - y^2$, xz, yz, and z^2 states). The extent of such an orbital mixing depends on the spin direction at a given Cu site. For example, consider the xy-plane spiral spin arrangement with repeat vector $q = 0.25$ shown in Figure 9b, where the spin moments at the spin sites 1–4 have the directions defined by

$$\begin{aligned}
&\text{Site 1: } \theta = 90^\circ,\ \phi = 90^\circ \\
&\text{Site 2: } \theta = 90^\circ,\ \phi = 0^\circ \\
&\text{Site 3: } \theta = 90^\circ,\ \phi = -90^\circ \\
&\text{Site 4: } \theta = 90^\circ,\ \phi = 180^\circ
\end{aligned} \tag{117}$$

The interaction matrix elements to consider are $\langle xy|\hat{H}^{sc}_{SO}|j\rangle$, where j = xz, yz, $x^2 - y^2$, or z^2. For the spin directions of eq. (117), the $\hat{H}^{sc}_{SO}$ operators at the spin sites 1–4 are given by

$$\begin{aligned}
&\text{Site 1: } \hat{H}^{sc}_{SO} = \frac{i}{2}\lambda\hat{S}_n(-\hat{L}_+ + \hat{L}_-) \\
&\text{Site 2: } \hat{H}^{sc}_{SO} = \frac{1}{2}\lambda\hat{S}_n(\hat{L}_+ + \hat{L}_-) \\
&\text{Site 3: } \hat{H}^{sc}_{SO} = \frac{i}{2}\lambda\hat{S}_n(\hat{L}_+ - \hat{L}_-) \\
&\text{Site 4: } \hat{H}^{sc}_{SO} = \frac{1}{2}\lambda\hat{S}_n(\hat{L}_+ + \hat{L}_-)
\end{aligned} \tag{118}$$

Then, from the angular dependences of the d-states shown in eq. (110), the nonzero $\langle xy|\hat{H}^{sc}_{SO}|j\rangle$ elements at the spin sites 1–4 are found to be as follows:

$$\begin{aligned}
&\text{Site 1: } \langle xy|\hat{H}^{sc}_{SO}|yz\rangle \\
&\text{Site 2: } \langle xy|\hat{H}^{sc}_{SO}|xz\rangle \\
&\text{Site 3: } \langle xy|\hat{H}^{sc}_{SO}|yz\rangle \\
&\text{Site 4: } \langle xy|\hat{H}^{sc}_{SO}|xz\rangle
\end{aligned} \tag{119}$$

Namely, the nature of the orbital mixing at each spin site depends on its spin orientation.

It is important to note that each d state of a given Cu site has the 2p orbitals of its surrounding O atoms combined out-of-phase with the Cu 3d orbital. The orbital mixing induced by the spin-orbit coupling gives rise eventually to the asymmetric electron density distribution largely on the O sites,[33] and to nonzero electric polarization.

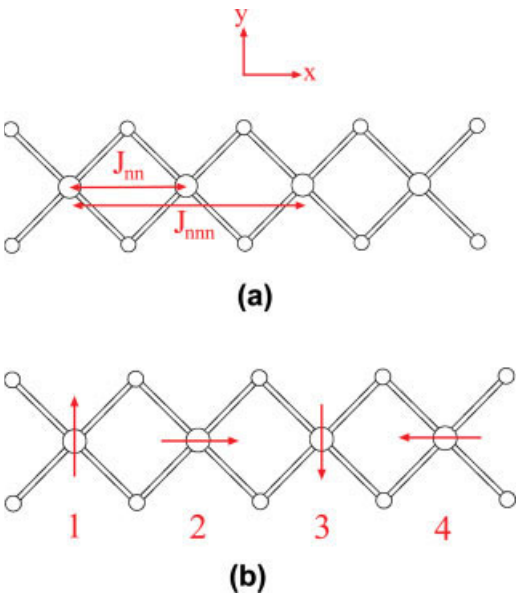

Figure 9. (a) Nearest-neighbor and next-nearest-neighbor spin exchange interactions (J_{nn} and J_{nnn}, respectively) of a CuO_2 ribbon chain. (b) Spiral spin in the *xy*-plane with repeat vector $q = 0.25$.

Uniaxial Magnetism as a Consequence of Electron Correlation, Direct Metal–Metal Bonding, Ferromagnetism, and Spin-Orbit Coupling

As discussed in "High-spin d^6 ions at trigonal prism and linear two coordinate sites" section, the uniaxial magnetic property of $Ca_3Co_2O_6$ makes one conclude that at each CoO_6 trigonal prism site a down-spin d-electron must occupy the degenerate $l = \pm 2$ level (Figs. 5b and 5c) rather than the $l = 0$ level (Fig. 5a).[3] For a high-spin Co^{3+} (d^6) ion at an *isolated* trigonal prism site, the configuration $(\uparrow l = 0)^1(\uparrow l = \pm 2)^1(\uparrow l = \pm 1)^1(\downarrow l = \pm 2)^1$, hereafter referred to as $[\uparrow](\downarrow l = \pm 2)^1$, is less favorable energetically than the configuration $(\uparrow l = 0)^1(\uparrow l = \pm 2)^1(\uparrow l = \pm 1)^1(\downarrow l = 0)^1$, hereafter referred to as $[\uparrow](\downarrow l = 0)^1$. In each Co_2O_6 chain, there occur direct metal-metal interactions between the $l = 0$ orbitals (i.e., the z^2 orbitals) of adjacent Co^{3+} ions. If the z^2 orbitals of the trigonal prism and the octahedral sites are each doubly occupied (Fig. 10a), the direct metal–metal interactions lead to a net destabilization because, for every adjacent pairs of trigonal prism and octahedral sites, the interaction between the z^2 orbitals is a two-orbital four-electron destabilizing interaction.[37] To get rid of this destabilization, electron removal is necessary from the z^2 orbital of either the octahedral or the trigonal prism site. As discussed below, the latter is achieved as a consequence of direct metal-metal interaction, electron correlation, ferromagnetism and spin-orbit coupling.

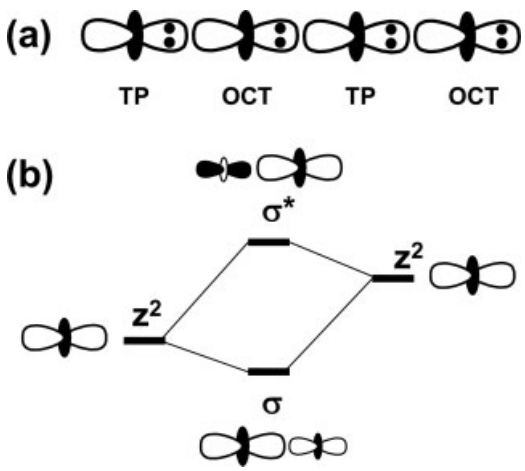

Figure 10. (a) Arrangement of the doubly-filled z^2 orbitals at the trigonal prism (TP) and octahedral (OCT) sites in each Co_2O_6 chain of $Ca_3Co_2O_6$. (b) Sigma-bonding and σ-antibonding levels (σ and σ^*, repectively) resulting from the z^2 orbitals of adjacent TP and OCT sites in case when the z^2 orbitals are different in energy.

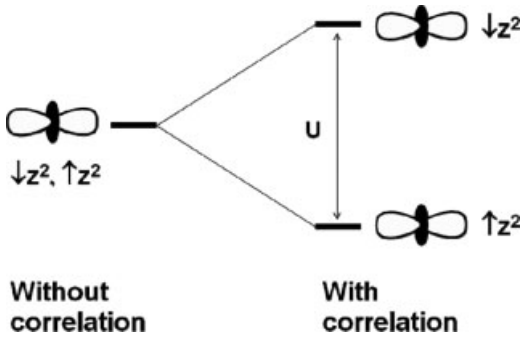

Figure 11. Up-spin and down-spin z^2 levels at each Co^{3+} site in each Co_2O_6 chain of $Ca_3Co_2O_6$ in the absence (left) and in the presence (right) of electron correlation, where U represents the on-site repulsion.

The direct metal-metal interaction between adjacent z^2 orbitals gives rise to σ-bonding and σ-antibonding levels (hereafter the σ and σ^* levels, respectively). When the z^2 levels are not degenerate, the σ level has a greater contribution from the z^2 level closer to it in energy, and so does the σ^* level (Fig.

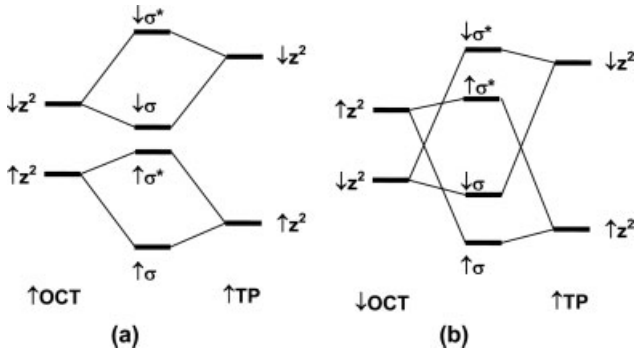

Figure 12. Orbital interactions between the up-spin and down-spin z^2 levels of adjacent trigonal prism (TP) and octahedral (OCT) sites in each Co_2O_6 chain of $Ca_3Co_2O_6$ for the case of (a) ferromagnetic and (b) antiferromagnetic spin arrangements. Here the σ and σ^* levels refer to the σ-bonding and σ-antibonding levels resulting from the z^2 orbitals of adjacent TP and OCT sites.

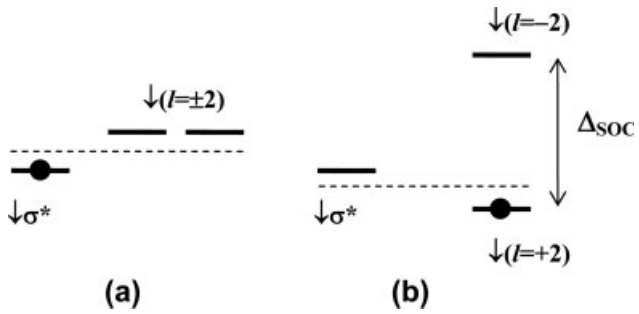

Figure 13. Comparison of the $\downarrow\sigma^*$ level between adjacent trigonal prism and octahedral sites with the $\downarrow l = \pm 2$ levels of the trigonal prism site in the Co_2O_6 chain of $Ca_3Co_2O_6$ in the (a) absence and (b) presence of spin-orbit coupling. Δ_{SOC} represents the energy split between the $\downarrow l = +2$ and $\downarrow l = -2$ levels induced by spin-orbit coupling. The $\downarrow l = +2$ level lies lower in energy than the $\downarrow l = -2$ level for the high-spin Co^{3+} (d^6) ion because the spin-orbit coupling constant λ is positive.

10b).[37] In the one-electron picture, in which electron correlation (i.e., electron–electron repulsion) is neglected, the up-spin and down-spin z^2 levels (hereafter the $\uparrow z^2$ and $\downarrow z^2$ levels, respectively) at each Co^{3+} site of $Ca_3Co_2O_6$ are the same. When electron correlation is taken into consideration, however, the $\uparrow z^2$ and $\downarrow z^2$ levels are split in energy by the amount of on-site repulsion U (Fig. 11). As depicted in Figure 12, the extent of this split is greater at the trigonal prism site than at the octahedral site, because the trigonal prism site has a high-spin Co^{3+} ion while the octahedral site has a low-spin Co^{3+} ion. If adjacent trigonal prism and octahedral sites have a ferromagnetic spin arrangement (e.g., both up-spins) as depicted in Figure 12a, the $\uparrow z^2$ level lies lower than the $\downarrow z^2$ level at each site. If adjacent trigonal prism and octahedral sites have an antiferromagnetic spin arrangement (e.g., down-spin at the octahedral site and up-spin at the trigonal prism site) as depicted in Figure 12b, the $\uparrow z^2$ level lies lower than the $\downarrow z^2$ level at the trigonal prism site but the opposite is true at the octahedral site. Consequently, the $\uparrow z^2$ orbitals of adjacent trigonal prism and octahedral sites have a smaller energy difference in the ferromagnetic than in the antiferromagnetic spin arrangement. Likewise, the $\downarrow z^2$ orbitals of adjacent trigonal prism and octahedral sites have a smaller energy difference in the ferromagnetic spin arrangement. As a result, the interaction between the $\downarrow z^2$ orbitals of adjacent trigonal prism and octahedral sites is stronger, and hence the resulting $\downarrow\sigma^*$ level lies higher in energy, in the ferromagnetic than in the antiferromagnetic spin arrangement.[37] The latter has important consequences. First principles density functional theory (DFT) calculations for the ferromagnetic state of $Ca_3Co_2O_6$ show [14c,d] that the Co^{3+} ion at each trigonal prism site has the electron configuration $[\uparrow](\downarrow l = 0)^1$ in the DFT calculations with electron-correlation (i.e., DFT+U calculations), but the electron configuration $[\uparrow](\downarrow l = \pm 2)^1$ in the DFT calculations with electron-correlation and spin-orbit coupling (i.e., DFT+U+SOC calculations). As illustrated in Figure 13, this finding originates from the fact that the spin-orbit coupling splits the degenerate $\downarrow l = \pm 2$ level of the trigonal prism site into the $\downarrow l = +2$ and $\downarrow l = -2$ levels. If the $\downarrow\sigma^*$ level lies high in energy, which occurs for the ferromagnetic spin arrangement within each Co_2O_6 chain, the level $\downarrow l = +2$ can be lowered below the $\downarrow\sigma^*$ level (Fig. 13) so that the level $\downarrow l = +2$ becomes occupied while the $\downarrow\sigma^*$ level becomes empty. As can be deduced from Figures 10b and 12a, the major contributor of the $\downarrow\sigma^*$ level is the $\downarrow z^2$ orbital of the trigonal prism site so that the electron removal from the $\downarrow\sigma^*$ level amounts largely to that from the $\downarrow z^2$ orbital of the trigonal prism site. To a first approximation, therefore, the electron configuration of the trigonal prism site in the ferromagnetic state is described by $[\uparrow](\downarrow l = +2)^1$, which is a consequence of direct metal–metal interaction, electron correlation and spin-orbit coupling. The electron configuration $[\uparrow](\downarrow l = +2)^1$ at each trigonal site makes each Co_2O_6 chain uniaxial in magnetic property. As a result of the electron removal from the σ-antibonding level, $\downarrow\sigma^*$, the direct metal-metal interaction becomes net bonding. In other words, the uniaxial magnetism in $Ca_3Co_2O_6$ represents a cooperative effect of direct metal–metal bonding, electron correlation, ferromagnetism and spin-orbit coupling.

Concluding Remarks

As described in the previous sections, a key to understanding the magnetic properties of discrete and extended compounds with unpaired spins is to know their ground and low-lying excited states. The nature of these magnetic states can be strongly affected by spin-orbit coupling. In this review we surveyed quantum mechanical descriptions on how to describe magnetic properties associated with spin-orbit coupling. It is hoped that this review will serve as a stepping stone toward comprehending how to think about spin orbit coupling and its applications.

Appendix: Derivation of eq. (108)

As discussed in http://en.wikipedia.org/wiki/Rotation_operator, the spin operators $\hat{S}_x$, $\hat{S}_y$, and $\hat{S}_z$ of a given coordinate system are transformed into a different set of spin operators $\hat{S}_{x'}$, $\hat{S}_{y'}$, and $\hat{S}_z'$ when the coordinate system is rotated. The two sets of spin operators are related as

$$\begin{aligned} \hat{S}_{x'} &= D\hat{S}_x D^{-1} \\ \hat{S}_{y'} &= D\hat{S}_y D^{-1}, \\ \hat{S}_{z'} &= D\hat{S}_z D^{-1} \end{aligned} \tag{A1}$$

where D is an appropriate spin rotation operator defined in terms of the azimuthal and polar angles (θ and ϕ, respectively) of the magnetization direction $\vec{n}(\theta, \phi)$ in the rectangular crystal coordinate system. Note that we define $\hat{S}_{z'} = \hat{S}_n$.

For simplicity of our derivation of eq. (108), we first assume that $\phi = 0$, i.e., the spin lies in the xz-plane and rotates around the y-axis. In this case, the rotation matrix D is written as

$$D = \begin{bmatrix} \cos\frac{\theta}{2} & -\sin\frac{\theta}{2} \\ \sin\frac{\theta}{2} & \cos\frac{\theta}{2} \end{bmatrix}, \tag{A2}$$

which is unitary so that the transpose of D is equal to D^{-1}. The matrix representations of the spin operators $\hat{S}_i$ ($i = x, y, z$) for a

given coordinate system can be expressed by using the Pauli matrices

$$\boldsymbol{S}_i = \frac{1}{2}\sigma_i \quad (i = x, y, z) \tag{A3}$$

where

$$\sigma_x = \begin{bmatrix} 0 & 1 \\ 1 & 0 \end{bmatrix}, \quad \sigma_y = \begin{bmatrix} 0 & -i \\ i & 0 \end{bmatrix}, \quad \sigma_z = \begin{bmatrix} 1 & 0 \\ 0 & -1 \end{bmatrix}, \tag{A4}$$

and

$$\sigma_+ = \sigma_x + i\sigma_y, \quad \sigma_- = \sigma_x - i\sigma_y. \tag{A5}$$

From eq. (A1), we obtain

$$\begin{aligned} \hat{S}_x &= D^{-1}\hat{S}_{x'}D \\ \hat{S}_y &= D^{-1}\hat{S}_{y'}D, \\ \hat{S}_z &= D^{-1}\hat{S}_{z'}D \end{aligned} \tag{A6}$$

so that the combination of eqs. (A2) and (A6) leads to

$$\begin{aligned} \hat{S}_x &= \hat{S}_{x'}\cos\theta + \hat{S}_{z'}\sin\theta \\ \hat{S}_y &= \hat{S}_{y'} \\ \hat{S}_z &= \hat{S}_{z'}\cos\theta - \hat{S}_{x'}\sin\theta \end{aligned} \tag{A7}$$

As shown in eq. (107), the term $\hat{L}\cdot\hat{S}$ is written as

$$\hat{L}\cdot\hat{S} = \hat{L}_z\hat{S}_z + \frac{1}{2}\hat{L}_+\hat{S}_- + \frac{1}{2}\hat{L}_-\hat{S}_+. \tag{A8}$$

Therefore, by using eq. (A7), the three components of $\hat{L}\cdot\hat{S}$ can be rewritten as

$$\begin{aligned} \hat{L}_z\hat{S}_z &= \hat{L}_z\left(\hat{S}_{z'}\cos\theta - \hat{S}_{x'}\sin\theta\right) \\ &= \hat{L}_z\left[\hat{S}_{z'}\cos\theta - \frac{1}{2}\left(\hat{S}_{+'} + \hat{S}_{-'}\right)\sin\theta\right], \\ &= \hat{S}_{z'}\hat{L}_z\cos\theta + \frac{1}{2}\hat{S}_{+'}\hat{L}_z(-\sin\theta) + \frac{1}{2}\hat{S}_{-'}\hat{L}_z(-\sin\theta) \end{aligned} \tag{A9}$$

$$\begin{aligned} \frac{1}{2}\hat{L}_+\hat{S}_- &= \frac{1}{2}\hat{L}_+\left(\hat{S}_x - i\hat{S}_y\right) \\ &= \frac{1}{2}\hat{L}_+\left[\hat{S}_{x'}\cos\theta + \hat{S}_{z'}\sin\theta - i\hat{S}_y\right] \\ &= \frac{1}{2}\hat{L}_+\left[\frac{1}{2}\left(\hat{S}_{+'} + \hat{S}_{-'}\right)\cos\theta + \hat{S}_{z'}\sin\theta - \frac{1}{2}\left(\hat{S}_{+'} - \hat{S}_{-'}\right)\right], \\ &= \hat{S}_{z'}\hat{L}_+\left(\frac{1}{2}\sin\theta\right) + \frac{1}{2}\hat{S}_{+'}\hat{L}_+\left(\frac{1}{2}\cos\theta - 1\right) \\ &\quad + \frac{1}{2}\hat{S}_{-'}\hat{L}_+\left(\frac{1}{2}\cos\theta + 1\right) \\ &= \hat{S}_{z'}\hat{L}_+\left(\frac{1}{2}\sin\theta\right) - \frac{1}{2}\hat{S}_{+'}\hat{L}_+\sin^2\frac{\theta}{2} + \frac{1}{2}\hat{S}_{-'}\hat{L}_+\cos^2\frac{\theta}{2} \end{aligned} \tag{A10}$$

$$\begin{aligned} \frac{1}{2}\hat{L}_-\hat{S}_+ &= \frac{1}{2}\hat{L}_-\left(\hat{S}_x + i\hat{S}_y\right) \\ &= \frac{1}{2}\hat{L}_-\left[\hat{S}_{x'}\cos\theta + \hat{S}_{z'}\sin\theta + i\hat{S}_y\right] \\ &= \frac{1}{2}\hat{L}_-\left[\frac{1}{2}\left(\hat{S}_{+'} + \hat{S}_{-'}\right)\cos\theta + \hat{S}_{z'}\sin\theta + \frac{1}{2}\left(\hat{S}_{+'} - \hat{S}_{-'}\right)\right]. \\ &= \hat{S}_{z'}L'_-\left(\frac{1}{2}\sin\theta\right) + \frac{1}{2}\hat{S}_{+'}\hat{L}_-\left(\frac{1}{2}\cos\theta + 1\right) \\ &\quad + \frac{1}{2}\hat{S}_{-'}\hat{L}_-\left(\frac{1}{2}\cos\theta - 1\right) \\ &= \hat{S}_{z'}\hat{L}_-\left(\frac{1}{2}\sin\theta\right) + \frac{1}{2}\hat{S}_{+'}\hat{L}_-\cos^2\frac{\theta}{2} - \frac{1}{2}\hat{S}_{-'}\hat{L}_-\sin^2\frac{\theta}{2} \end{aligned} \tag{A11}$$

Finally, by combining eqs. (A8)–(A10), we obtain the following expression of $\hat{L}\cdot\hat{S}$ for the case of $\phi = 0$.

$$\begin{aligned} \hat{L}\cdot\hat{S} = S_{z'}&\left(\hat{L}_-\cos\theta + \frac{1}{2}\hat{L}_+\sin\theta + \frac{1}{2}\hat{L}_-\sin\theta\right) \\ &+ \frac{1}{2}\hat{S}_{+'}\left(-\hat{L}_z\sin\theta - \hat{L}_+\sin^2\frac{\theta}{2} + \hat{L}_-\cos^2\frac{\theta}{2}\right) \\ &+ \frac{1}{2}\hat{S}_{-'}\left(-\hat{L}_z\sin\theta + \hat{L}_+\cos^2\frac{\theta}{2} - \hat{L}_-\sin^2\frac{\theta}{2}\right) \end{aligned} \tag{A12}$$

In this expression it is important to notice that the orbital angular momentum operators are defined in terms of the un-rotated coordinate system, but the spin angular momentum operators in terms of the rotated coordinate system. As long as this is understood, the primes of the spin operators signaling the rotated coordinate system can be dropped to simplify the expression.

Consider now the derivation of eq. (108) for the general case of $\phi \neq 0$. In this case, the rotation operator D is written as the product of two rotation operators

$$D = D_\phi D_\theta = \begin{bmatrix} e^{-i\frac{\phi}{2}} & 0 \\ 0 & e^{i\frac{\phi}{2}} \end{bmatrix}\begin{bmatrix} \cos\frac{\theta}{2} & -\sin\frac{\theta}{2} \\ \sin\frac{\theta}{2} & \cos\frac{\theta}{2} \end{bmatrix}, \tag{A13}$$

where D_θ and D_ϕ are the rotation matrices for the angles θ and ϕ, respectively. Using this operator and its inverse operator D^{-1}

$$D^{-1} = D_\theta^{-1}D_\phi^{-1} = \begin{bmatrix} \cos\frac{\theta}{2} & \sin\frac{\theta}{2} \\ -\sin\frac{\theta}{2} & \cos\frac{\theta}{2} \end{bmatrix}\begin{bmatrix} e^{i\frac{\phi}{2}} & 0 \\ 0 & e^{-i\frac{\phi}{2}} \end{bmatrix} \tag{A14}$$

into eq. (A6), one can obtain new relationships between the set of $\hat{S}_x$, $\hat{S}_y$, and $\hat{S}_z$ and that of $\hat{S}_{x'}$, $\hat{S}_{y'}$, and $\hat{S}_{z'}$. Then, by using the resulting relationships, it is straightforward to derive eq. (108) by following the steps similar to those of eqs. (A7)–(A12). However, there is an alternative method of deriving eq. (108) that is simpler and more elegant. It should be noted that the rotation of the spin momentum coordinate by ϕ is equivalent to the rotation of the orbital momentum coordinate by $-\phi$. Under the latter operation, the operators $\hat{L}_x$ and $\hat{L}_y$ are changed as

$$\begin{aligned}\hat{L}_x &\rightarrow \hat{L}_x\cos\phi + \hat{L}_y\sin\phi \\ \hat{L}_y &\rightarrow -\hat{L}_x\sin\phi + \hat{L}_y\cos\phi\end{aligned} \tag{A15}$$

As a consequence, the ladder operators $\hat{L}_\pm$ are transformed as

$$\begin{aligned}\hat{L}_\pm = \hat{L}_x \pm i\hat{L}_y &\rightarrow \left(\hat{L}_x\cos\phi + \hat{L}_y\sin\phi\right) \pm i\left(-\hat{L}_x\sin\phi + \hat{L}_y\cos\phi\right) \\ &= \left(\hat{L}_x \pm i\hat{L}_y\right)(\cos\phi \pm i\,\sin\phi) = \hat{L}_\pm e^{\pm i\phi}\end{aligned} \tag{A16}$$

Then, eq. (A12) becomes eq. (108) when the operators $\hat{L}_\pm$ are replaced with the rotated operators $\hat{L}_\pm e^{\mp i\phi}$.

References

1. Mabbs, F. E.; Machin, D. J. Magnetism and Transition Metal Complexes; Long Chapman and Hall: London, 1973.
2. Dunn, T. M. Trans Faraday Soc 1961, 57, 1441.
3. Dai, D.; Whangbo, M.-H. Inorg Chem 2005, 44, 4407.
4. Carson, E. H.; Spence, R. D. J Chem Phys 1956, 24, 471.
5. Orgel, L. E. J Chem Phys 1955, 23, 1004.
6. Pryce, M. H. L. Proc Phys Soc (London) A 1950, 63, 25.
7. Lines, M. E. Phys Rev 1963, 131, 546.
8. Fjellvåg, H.; Gulbrandsen, E.; Aasland, S.; Olsen, A.; Hauback, B. J Solid State Chem 1996, 124, 190.
9. Kageyama, H.; Yoshimura, K.; Kosuge, K.; Azuma, M.; Takano, M.; Mitamura, H.; Goto, T. J. Phys Soc Jpn 1997, 66, 3996.
10. Maignan, A.; Michel, C.; Masset, A. C.; Martin, C.; Raveau, B. Eur Phys J B 2000, 15, 657.
11. Maignan, A.; Hardy, V.; Hébert, S.; Drillon, M.; Lees, M. R.; Petrenko, O.; Paul, D. Mc K.; Khomskii, D. J Mater Chem 2004, 14, 1231.
12. (a) Sampathkumaran, E. V.; Fujiwara, N.; Rayaprol, S.; Madhu, P. K.; Uwatoko, Y. Phys Rev B 2004, 70, 014437; (b) Hardy, V.; Lambert, S.; Lees, M. R.; Paul, D. Mc K. Phys Rev B 2003; 68, 014424.
13. Aasland, S.; Fjellvåg, H.; Hauback, B. Solid State Commun 1997, 101, 187.
14. (a) Whangbo, M.-H.; Dai, D.; Koo, H.-J.; Jobic, S. Solid State Commun 2003, 125, 413; (b) Eyert, V.; Laschinger, C.; Kopp, T.; Frésard, R. Chem Phys Lett 2004, 383, 249; (c) Wu, H.; Haverkort, M. W.; Hu, Z.; Khomskii, D. I.; Tjeng, L. H. Phys Rev Lett 2005, 95, 186401.
15. (a) LaPointe, A. M. Inorg Chim Acta 2003, 345, 359; (b) Viefhaus, T.; Schwarz, W.; Hübler, K.; Locke, K.; Weidlein, J. Z. Anorg Allg Chem 2001, 627, 715.
16. Reiff, W. M.; LaPointe A. M.; Witten, E. H. J Am Chem Soc 2004, 126, 10206.
17. (a) Ishiwata, S.; Wang, D.; Saito, T.; Takano, M. Chem Mater 2005, 17, 2789; (b) Mukuda, H.; Kitaoka, Y.; Ishiwata, S.; Saito, T.; Shimakawa, Y.; Harima, H.; Takano, M. J Phys Soc Jpn 2006, 75, 094715.
18. Lee, C.; Whangbo, M.-H.; Villesuzanne, A. Chem Mater 2007, 19, 2712.
19. Ikeda, N.; Ohsumi, H.; Ohwada, K.; Ishii, K.; Inami, T.; Kakurai, K.; Murakami, Y.; Yoshii, K.; Mori, S.; Horibe, Y. K. H. Nature 2005, 436, 1136.
20. Xiang, H. J.; Whangbo, M.-H. Phys Rev Lett 2007, 98, 246403.
21. Whangbo, M.-H.; Dai, D.; Lee, K.-S.; Kremer, R. K. Inorg Chem 2006, 18, 1268.
22. (a) Dzyaloshinsky, I. J Phys Chem Solids 1958, 4, 241; (b) Moriya, T. Phys Rev 1960, 120, 91; (c) Moriya, T. Phys Rev Lett 1960, 4, 228.
23. Anderson, P. W. Phys Rev 1959, 115, 2.
24. Whangbo, M.-H.; Koo, H.-J.; Dai, D. J Solid State Chem 2003, 176, 417.
25. Nagamiya, T.; Yosida, K.; Kubo, R. Adv Phys 1955, 4, 1.
26. Wang, X.; Wu, R.; Wang, D.-S.; Freeman, A. J. Phys Rev B 1996, 54, 61.
27. Kuneš, J.; Novák, P.; Diviš, M.; Oppeneer, P. M. Phys Rev B 2001, 63, 205111.
28. Erickson, A. S.; Misra, S.; Miller, G. J.; Gupta, R. R.; Schlesinger, Z.; Harrison, W. A.; Kim, J. M.; Fisher, I. R. Phys Rev Lett 2007, 99, 016404.
29. Xiang, H. J.; Whangbo, M.-H. Phys Rev B 2007, 75, 052407.
30. Lee, K.-W.; Pickett, W. E. EPL 2007, 80, 37008.
31. Tsujimoto, Y.; Tassel, C.; Hayashi, N.; Watanabe, T.; Kageyama, H.; Yoshimura, K.; Takano, M.; Ceretti, M.; Ritter, C.; Paulus, W. Nature 2007, 450, 1062.
32. Xiang, H. J.; Wei, S. H.; Whangbo, M.-H. Phys Rev Lett (submitted for publication).
33. Xiang, H. J.; Whangbo, M.-H. Phys Rev Lett 2007, 99, 257203.
34. Bursill, R.; Gehring, G. A.; Farnell, D. J. J.; Parkinson, J. B.; Xiang, T.; Zeng, C. J Phys: Condens Matter 1995, 7, 8605.
35. Cheong, S.-W.; Mostovoy, M. Nat Mat 2007, 6, 13.
36. Katsura, H.; Nagaosa, N.; Balatsky, A. Phys Rev Lett 2005, 95, 057205.
37. Albright, T. A.; Burdett, J. K.; Whangbo, M.-H. Orbital Interactions in Chemistry; Wiley: New York, 1985.